

SCALING FOR ICING WIND TUNNEL TESTS AND VALIDATION WITH
NUMERICAL SIMULATIONS

A THESIS SUBMITTED TO
THE GRADUATE SCHOOL OF NATURAL AND APPLIED SCIENCES
OF
MIDDLE EAST TECHNICAL UNIVERSITY

BY

GİZEM ÖZBEK YANMAZ

IN PARTIAL FULFILLMENT OF THE REQUIREMENTS
FOR
THE DEGREE OF MASTER OF SCIENCE
IN
AEROSPACE ENGINEERING

SEPTEMBER 2019

Approval of the thesis:

**SCALING FOR ICING WIND TUNNEL TESTS AND VALIDATION WITH
NUMERICAL SIMULATIONS**

submitted by **GİZEM ÖZBEK YANMAZ** in partial fulfillment of the requirements
for the degree of **Master of Science in Aerospace Engineering Department, Middle
East Technical University** by,

Prof. Dr. Halil Kalıpçılar
Dean, Graduate School of **Natural and Applied Sciences**

Prof. Dr. İsmail Hakkı Tuncer
Head of Department, **Aerospace Engineering**

Prof. Dr. Serkan Özgen
Supervisor, **Aerospace Engineering, METU**

Examining Committee Members:

Prof. Dr. İsmail Hakkı Tuncer
Aerospace Engineering, METU

Prof. Dr. Serkan Özgen
Aerospace Engineering, METU

Prof. Dr. Zafer Dursunkaya
Mechanical Engineering, METU

Prof. Dr. Yusuf Özyörük
Aerospace Engineering, METU

Prof. Dr. Hasan Umur Akay
Mechanical Engineering, Atılım University

Date: 09.09.2019

I hereby declare that all information in this document has been obtained and presented in accordance with academic rules and ethical conduct. I also declare that, as required by these rules and conduct, I have fully cited and referenced all material and results that are not original to this work.

Name, Surname: Gizem Özbek Yanmaz

Signature:

ABSTRACT

SCALING FOR ICING WIND TUNNEL TESTS AND VALIDATION WITH NUMERICAL SIMULATIONS

Özbek Yanmaz, Gizem
Master of Science, Aerospace Engineering
Supervisor: Prof. Dr. Serkan Özgen

September 2019, 104 pages

Icing is one of the most dangerous hazards to be encountered by air vehicles in flight. Ice accretion, particularly on control surfaces, wings and flight data sensors usually degrades both performance and operational safety of air vehicles. Thus, it has become important in the design and certification phases of system development to evaluate performance degradation because of icing. Icing wind tunnel testing is the most convenient method considering feasibility, cost and safety. However, when full-size model is too large for a given facility or when the desired test conditions are out of the operating capability of the facility, a scaling method that produces scaled ice accretions over a wide range of test conditions and that can be applied to a variety of icing testing situations is needed. The scaling method shall be validated before the icing wind tunnel testing for reliability and validity of the tests. This work illustrates a scaling method for size scaling and test-condition scaling that is based on similitudes of geometry, flow field, droplet trajectory, water catch, energy balance and surface water dynamics. Icing analyses are performed for full-size and scaled conditions using an in-house icing code AEROMSICE-2D and a CFD tool ANSYS® Fluent 18.0 and in-flight icing code FENSAP-ICE. The ice accretions obtained by analyses are verified with experimental data available in the literature. Furthermore, the scaling method is tested for geometry scaling and velocity scaling at several icing conditions.

Keywords: In-flight Icing, Icing Scaling, Icing Similitude, Icing Simulations, Icing Test Condition Scaling

ÖZ

BUZLANMA RÜZGAR TÜNELİ TESTLERİNDE ÖLÇEKLENDİRME VE SAYISAL ANALİZLERLE DOĞRULANMASI

Özbek Yanmaz, Gizem
Yüksek Lisans, Havacılık ve Uzay Mühendisliği
Tez Danışmanı: Prof. Dr. Serkan Özgen

Eylül 2019, 104 sayfa

Buzlanma, uçuş sırasında hava araçlarının karşılaştığı en tehlikeli problemlerden biridir. Özellikle kontrol yüzeylerinde, kanatlarda ve uçuş veri sensörlerinde buz birikmesi hava araçlarının hem performansını hem de çalışma güvenliğini kötü yönde etkiler. Bu nedenle, buzlanma nedeniyle meydana gelen performans düşüşünü değerlendirmek, sistem geliştirme tasarım ve sertifikalandırma aşamalarında önem kazanmıştır. Buzlanma rüzgâr tüneli testi, buzlanma tahmini için, fizibilite, maliyet ve güvenlik açısından en uygun yöntemdir. Bununla birlikte, model tünel için çok büyük veya istenen test koşulları tünelin işletme kapasitesinin dışında olduğunda, ölçeklendirilmiş durum için referans durumla aynı buz şeklinin elde edildiği bir ölçeklendirme yöntemi kullanılması gerekir. Testlerin güvenilirliği ve geçerliliği için buzlanma rüzgâr tüneli testinden önce, ölçeklendirme metodu doğrulanmalıdır. Bu çalışmada, geometri, akış alanı, damlacık yörüngesi, toplam yakalanan su, enerji dengesi ve yüzey-su dinamiklerini benzeten bir ölçeklendirme yöntemi kullanılmıştır. Bu yöntem hem model boyutu ölçeklendirme için hem de test koşullarını ölçeklendirmek için kullanılabilir. Buzlanma analizleri, in-house buzlanma kodu AEROMSICE-2D ve ticari bir HAD aracı olan ANSYS® Fluent 18.0 ve buzlanma kodu FENSAP-ICE kullanılarak referans ve ölçeklendirilmiş koşullar için gerçekleştirilmiştir. Analizlerle elde edilen buz şekilleri literatürde mevcut deneysel

veriler ve numerik analiz sonuçları ile karşılaştırılmıştır. Ölçeklendirme yöntemi, çeşitli buzlanma koşullarında geometri ölçeklendirmesi ve hız ölçeklendirmesi için test edilmiştir.

Anahtar Kelimeler: Uçuş Esnasında Buzlanma, Buzlanma Ölçeklendirmesi, Buzlanma Benzetimi, Buzlanma Test Koşulları Benzetimi

To my love and to my family,

ACKNOWLEDGEMENTS

I would like to express my gratitude to my supervisor Prof. Dr. Serkan Özgen for his guidance, support and sharing his knowledge and experience generously with me. Having chance to work with him gave me better perspective and improved me academically.

The thesis is supported by TÜBİTAK-SAGE (The Scientific and Technological Research Council of Turkey Defense Industries Research and Development Institute). I would like to thank TÜBİTAK-SAGE administration for allowing me perform the thesis study and providing resources. I would also like to thank all my colleagues at TÜBİTAK-SAGE Aerodynamics Division, especially Hasan Başar Bolat and Ufuk Başlamışli for their valuable ideas, help and support.

I would like to express my appreciation to my loving husband and best friend Denis Denizhan Yanmaz, to my dear parents Meryem and Malik Özbek and one and only sister Beren Özbek who were always there for me when I need them, always believe in me, support and love me unconditionally.

TABLE OF CONTENTS

ABSTRACT	v
ÖZ	vii
ACKNOWLEDGEMENTS	x
TABLE OF CONTENTS	xi
LIST OF TABLES	xiv
LIST OF FIGURES	xvii
LIST OF ABBREVIATIONS	xx
LIST OF SYMBOLS	xxi
CHAPTERS	
1. INTRODUCTION	1
1.1. Motivation	1
1.2. Literature Survey	5
1.3. Objectives	8
2. IN-FLIGHT ICING PHYSICS	9
2.1. Ice Formation	9
2.2. Factors Affecting Icing	10
2.2.1. Liquid Water Content (LWC)	11
2.2.2. Droplet Size	11
2.2.3. Temperature	12
2.2.4. Size of the Object	13
2.2.5. Airspeed	14
2.2.6. Exposure Time	14

3. ICING PREDICTION	15
3.1. Flow Field Solution.....	15
3.1.1. AEROMSICE-2D.....	15
3.1.2. FENSAP-ICE	16
3.2. Droplet Trajectories and Collection Efficiencies.....	17
3.2.1. AEROMSICE-2D.....	17
3.2.2. FENSAP-ICE	20
3.3. Thermodynamic Analysis	22
3.3.1. AEROMSICE-2D.....	22
3.3.2. FENSAP-ICE	25
3.4. Ice Accretion Modeling	25
3.4.1. AEROMSICE-2D.....	25
3.4.2. FENSAP-ICE	30
4. ICING SIMILITUDE ANALYSIS	37
4.1. Geometric similarity	37
4.2. Flow field similarity.....	38
4.3. Droplet trajectory similarity.....	39
4.4. Water catch similarity	40
4.5. Energy balance similarity.....	40
4.6. Surface-water dynamics similarity.....	43
5. ANALYSES	45
5.1. Analysis Set-up	45
5.1.1. AEROMSICE-2D.....	45
5.1.2. FENSAP-ICE	47

5.1.2.1. Flow solution.....	47
5.1.2.2. Droplet trajectories.....	48
5.1.2.3. Ice formation.....	52
5.2. Similitude Method.....	56
6. RESULTS AND DISCUSSION.....	61
6.1. CONCLUSION.....	93
REFERENCES.....	95
APPENDICES	
A. Mesh and Flow Solution Checks.....	99

LIST OF TABLES

TABLES

Table 5.1. Input parameters for AEROMSICE-2D	46
Table 6.1. Case 27 icing conditions for reference and scaled cases in reference [37]	64
Table 6.2. Case 27 scaling parameters for reference and scaled cases in reference [37]	64
Table 6.3. Case 28 icing conditions for reference and scaled cases in reference [37]	66
Table 6.4. Case 28 scaling parameters for reference and scaled cases in reference [37]	66
Table 6.5. Case 29 icing conditions for reference and scaled cases in reference [37]	68
Table 6.6. Case 29 scaling parameters for reference and scaled cases in reference [37]	68
Table 6.7. Case 30 icing conditions for reference and scaled cases in reference [37]	70
Table 6.8. Case 30 scaling parameters for reference and scaled cases in reference [37]	70
Table 6.9. Case 31 icing conditions for reference and scaled cases in reference [37]	71
Table 6.10. Case 31 scaling parameters for reference and scaled cases in reference [37].....	71
Table 6.11. Case 32 icing conditions for reference and scaled cases in reference [37]	73
Table 6.12. Case 32 scaling parameters for reference and scaled cases in reference [37].....	73

Table 6.13. Case 33 icing conditions for reference and scaled cases in reference [37]	75
Table 6.14. Case 33 scaling parameters for reference and scaled cases in reference [37]	75
Table 6.15. Case 34 icing conditions for reference and scaled cases in reference [37]	77
Table 6.16. Case 34 scaling parameters for reference and scaled cases in reference [37]	77
Table 6.17. Case 35 icing conditions for reference and scaled cases in reference [37]	79
Table 6.18. Case 35 scaling parameters for reference and scaled cases in reference [37]	79
Table 6.19. Case 36 icing conditions for reference and scaled cases in reference [37]	81
Table 6.20. Case 36 scaling parameters for reference and scaled cases in reference [37]	81
Table 6.21. Case 39 icing conditions for reference and scaled cases in reference [37]	83
Table 6.22. Case 39 scaling parameters for reference and scaled cases in reference [37]	83
Table 6.23. Case 40 icing conditions for reference and scaled cases in reference [37]	85
Table 6.24. Case 40 scaling parameters for reference and scaled cases in reference [37]	85
Table 6.25. Case 41 icing conditions for reference and scaled cases in reference [37]	87
Table 6.26. Case 41 scaling parameters for reference and scaled cases in reference [37]	87
Table 6.27. Case 42 icing conditions for reference and scaled cases in reference [37]	89

Table 6.28. Case 42 scaling parameters for reference and scaled cases in reference [37].....	89
Table 6.29. Case * icing conditions.....	91
Table 6.30. Case * scaling parameters.....	91

LIST OF FIGURES

FIGURES

Figure 1.1. In-flight icing tests [17]	2
Figure 1.2. Icing tests in simulated clouds produced by icing tanker [9]	3
Figure 1.3. Ice accretion on a wing in an icing wind tunnel [18]	4
Figure 2.1. Rime ice [30]	9
Figure 2.2. Glaze (clear) ice [30]	10
Figure 2.3. Total collection efficiencies [30]	11
Figure 2.4. Effect LWC on ice accretion [30].....	11
Figure 2.5. Effect of droplet size on ice accretion [30].....	12
Figure 2.6. Effect of droplet size on collection efficiency [27]	12
Figure 2.7. Effect of total temperature on ice accretion [30]	13
Figure 2.8. Effect of airframe size on collection efficiency [27].....	13
Figure 2.9. Effect of airspeed on collection efficiency [27]	14
Figure 3.1. Definition of collection efficiency [28]	20
Figure 3.2. Module interactions in FENSAP-ICE [5].....	30
Figure 3.3. Ice accretion in ICE-3D [2]	31
Figure 3.4. Ice accretion in ICE-3D [2]	35
Figure 5.1. FENSAP-ICE software DROP3D Model Tab.....	49
Figure 5.2. FENSAP-ICE software DROP3D Conditions Tab	50
Figure 5.3. FENSAP-ICE software DROP3D Boundaries Tab.....	51
Figure 5.4. FENSAP-ICE software DROP3D Solver Tab.....	51
Figure 5.5. FENSAP-ICE software DROP3D Out Tab	52
Figure 5.6. FENSAP-ICE software ICE3D Model Tab.....	53
Figure 5.7. FENSAP-ICE software ICE3D Conditions Tab.....	53
Figure 5.8. FENSAP-ICE software ICE3D Boundaries Tab	55
Figure 5.9. FENSAP-ICE software ICE3D Solver Tab.....	55

Figure 5.10. FENSAP-ICE software ICE3D Out Tab	56
Figure 5.11. Flow chart for similitude method	57
Figure 6.1. Case 27 Cp distributions, collection efficiencies and ice shapes obtained by analyses and experiments in reference [37] for NACA0012 airfoil at 4° AOA...	64
Figure 6.2. Case 28 Cp distributions, collection efficiencies and ice shapes obtained by analyses and experiments in reference [37] for NACA0012 airfoil at 4° AOA...	66
Figure 6.3. Case 29 Cp distributions, collection efficiencies and ice shapes obtained by analyses and experiments in reference [37] for NACA0012 airfoil at 4° AOA...	68
Figure 6.4. Case 30 Cp distributions, collection efficiencies and ice shapes obtained by analyses and experiments in reference [37] for NACA0012 airfoil at 4° AOA...	70
Figure 6.5. Case 31 Cp distributions, collection efficiencies and ice shapes obtained by analyses and experiments in reference [37] for NACA0012 airfoil at 4° AOA...	71
Figure 6.6. Case 32 Cp distributions, collection efficiencies and ice shapes obtained by analyses and experiments in reference [37] for NACA0012 airfoil at 4° AOA...	73
Figure 6.7. Case 33 Cp distributions, collection efficiencies and ice shapes ice shapes obtained by analyses and experiments in reference [37] for NACA0012 airfoil at 4° AOA.....	75
Figure 6.8. Case 34 Cp distributions, collection efficiencies and ice shapes obtained by analyses and experiments in reference [37] for NACA0012 airfoil at 4° AOA...	77
Figure 6.9. Case 35 Cp distributions, collection efficiencies and ice shapes obtained by analyses and experiments in reference [37] for NACA0012 airfoil at 4° AOA...	79
Figure 6.10. Case 36 Cp distributions, collection efficiencies and ice shapes obtained by analyses and experiments in reference [37] for NACA0012 airfoil at 4° AOA...	81
Figure 6.11. Case 39 Cp distributions, collection efficiencies and ice shapes obtained by analyses in reference [37] for NACA0012 airfoil at 8° AOA	83
Figure 6.12. Case 40 Cp distributions, collection efficiencies and ice shapes obtained by analyses and experiments in reference [37] for SA13112 airfoil at 10° AOA.....	85
Figure 6.13. Case 41 Cp distributions, collection efficiencies and ice shapes obtained by analyses and experiments in reference [37] for SA13112 airfoil at 0° AOA.....	87

Figure 6.14. Case 42 Cp distributions, collection efficiencies and ice shapes obtained by analyses in reference [37] for SA13112 airfoil at 0° AOA.....	89
Figure 6.15. Case * ice shapes obtained by analyses for SA13112 airfoil at 0° AOA	91
Figure A.1. NACA0012 Mesh	100
Figure A.2. SA13112 Mesh	100
Figure A.3. Case 32 y^+ distributions, NACA0012, $c_{reference}=0.53$ m, $c_{scaled}=0.265$ m	101
Figure A.4. (a) Case 40 y^+ distributions, SA13112, $c_{reference}=0.6$ m, $c_{scaled}=1.2$ m, (b) Case * y^+ distributions, SA13112, $c_{reference}=0.533$ m, $c_{scaled}=0.8$ m	101
Figure A.5. NACA0012, mesh and velocity vectors in boundary layer for Case 32, $c=0.53$ m.....	102
Figure A.6. NACA0012, mesh and velocity vectors in boundary layer for Case 32, $c=0.265$ m.....	102
Figure A.7. SA13112, mesh and velocity vectors in boundary layer for Case 40, $c=0.6$ m.....	103
Figure A.8. SA13112, mesh and velocity vectors in boundary layer for Case 40, $c=1.2$ m.....	103
Figure A.9. SA13112, mesh and velocity vectors in boundary layer for Case *, $c=0.533$ m.....	104
Figure A.10. SA13112, mesh and velocity vectors in boundary layer for Case *, $c=0.8$ m.....	104

LIST OF ABBREVIATIONS

ABBREVIATIONS

AEDC	Arnold Engineering Development Center
AERTS	Adverse Environment Rotor Test Stand
DRA	Defence Research Agency
EASA	European Aviation Safety Agency
ETF	Engine Test Facility
FAA	Federal Aviation Administration
FAR	Federal Aviation Regulation
LWC	Liquid Water Content
MVD	Median Volumetric Diameter
NACA	National Advisory Committee for Aeronautics
NASA	National Aeronautics and Space Administration
ONERA	Office National D'etudes Et de Recherches Aerospatiales
SLD	Supercooled Large Droplets

LIST OF SYMBOLS

SYMBOLS

A	area, m ²
A_c	accumulation parameter, dimensionless
AOA	angle of attack, °
b	relative heat factor, dimensionless
B	ice layer thickness, m
c	airfoil chord, m
C_D	drag coefficient of droplet, dimensionless
C_f	skin friction coefficient, dimensionless
C_p	constant-pressure specific heat of air, cal/g K
$C_{p,ws}$	specific heat of water on model surface, cal/g K
d	diameter, m
D	drag force on droplet, N
D_v	diffusivity of water vapor in air, m ² /s
e_0	saturation vapor pressure, 27.03
g	gravity vector, m/s ²
h	water film layer thickness, m
h_c	convective heat transfer coefficient, cal/ hr m ² K
h_G	gas-phase mass transfer coefficient, g/m ² s
k	thermal conductivity, cal/ hr m K
K	inertia parameter, dimensionless
K_0	modified inertia parameter, dimensionless
k_s	roughness height, m
L	characteristic length, m
L_e	Lewis number ($1/Pr$), dimensionless

L_E	latent heat of evaporation of water, J/K
L_F	latent heat of solidification of water, J/K
L_S	latent heat of sublimation of water, J/K
LWC	liquid water content, g/m ³
m	mass, kg
\dot{m}	mass flow rate, kg/s
$\dot{m}_{e,s}$	evaporating or sublimating mass flow rate, kg/s
\dot{m}_i	instantaneous mass accumulation rate of ice, kg/s
\dot{m}_{in}	runback mass flow rate, kg/s
M	Mach number, dimensionless
n	freezing fraction, dimensionless
n_0	freezing fraction at stagnation, dimensionless
P	pressure, Pa
P_w	vapor pressure of water over liquid water, Pa
P_{ww}	vapor pressure of water in the atmosphere, Pa
Pr	Prandtl number, dimensionless
Q_a	surface heat gain due to aerodynamic heating, W/m ²
Q_c	surface heat loss due to convection, W/m ²
Q_d	cooling from incoming droplets, W/m ²
Q_e	surface heat loss from evaporation, W/m ²
Q_{in}	surface heat gain due to incoming run-back water, W/m ²
Q_k	surface heat gain from kinetic energy of water droplets, W/m ²
Q_l W/m ²	surface heat gain from release of latent heat of solidification, W/m ²
Q_r	surface heat loss from radiation, W/m ²
Q_s	surface heat loss from sublimation, W/m ²
r	adiabatic recovery factor, dimensionless
R_a	gas constant for air, N m/g K

Re	Reynolds number, dimensionless
s	circumferential distance along airfoil, m
Sc	Schmidt number, dimensionless
St	Stanton number, dimensionless
T	static temperature, K
t_{exp}	icing time, s
V	free-stream velocity, m/s
V_x, V_y	components of velocity vector, m/s
x, y	Cartesian coordinates, m
x_d, y_d	components of droplet position vector, m
\dot{x}_d, \dot{y}_d	components of droplet velocity vector, m/s
\ddot{x}_d, \ddot{y}_d	components of droplet acceleration vector, m/s ²
We	Weber number, dimensionless
α	angle of attack, water volume fraction; °, dimensionless
β	catch efficiency, dimensionless
β_0	catch efficiency at stagnation, dimensionless
γ	ratio of specific heats for air, angle between droplet and freestream velocity vectors; 1.4, °
δ	median volumetric diameter, boundary layer thickness; μm , m
θ	air energy transfer parameter, momentum thickness; K, m
θ_w	temperature in water film layer, K
$\frac{\lambda}{\lambda_{Stokes}}$	droplet range parameter, dimensionless
μ	dynamic viscosity, Pa s
ν	kinematic viscosity, m ² /s
ρ	density, kg/m ³
Λ_f	latent heat of freezing, cal/g
Λ_v	latent heat of sublimation, cal/g
σ_{wa}	surface tension of water against air, N/m

χ_e	evaporation coefficient, m/s
χ_s	sublimation coefficient, m/s
ϕ	droplet energy transfer parameter, K
τ	shear stress, Pa

SUBSCRIPTS

0	on stagnation line
<i>a</i>	air
<i>d</i>	droplet
<i>f</i>	at the freezing point of water
<i>film</i>	at film, at wall/air/liquid-water/ice interface
<i>g</i>	glaze

CHAPTER 1

INTRODUCTION

1.1. Motivation

In-flight icing is one of the most hazardous incidents that air vehicles experience considering the consequences may be severe. Ice formation on aerodynamic surfaces, control surfaces and data gathering instruments reduces the performance and jeopardize operational safety of air vehicles. Susceptible parts of air vehicles for ice accretion are engine inlets, wings, control surfaces, rotors, sensors and probes. Icing of any of these may cause severe consequences. Engine inlet icing may cause distortion in the air flow; furthermore, the ice accreted on the inlet may break off and get in the compressor causing severe problems that may lead to engine stoppage. Icing on aerodynamic surfaces increases drag, decreases lift, stall speed is increased and stall angle is decreased. Results of icing on control surfaces such as tail wings are similar to aerodynamic surfaces, but more severe since the air vehicle may become uncontrollable. Icing on sensors and probes may lead to false readings that can cause erroneous decisions. The results of in-flight icing are mostly severe and sometimes fatal; thus, precautions must be taken before encountering any icing condition. Thus, it is of great importance to design and operate the air vehicle considering the limits and behavior against icing conditions. To be able to take precautions, the effects of icing should be taken into account starting from early design phases. In the design and certification phases of the air vehicle, evaluation of performance degradation because of icing and operational limits in icing conditions has become a necessary part of the process. Method of evaluating the effects of icing before actual flight is performed by computational analysis and tests. For early design phases, the results of computational analysis for in-flight icing are at acceptable accuracy and sufficient; however, for later design and certification phases, tests simulating the real flight icing

conditions must be performed to validate the computational results and examine the actual behavior of the air vehicle. Certification authorities, FAA and EASA, specify the meteorological icing certification conditions for an air vehicle to be certified to fly safely in Appendix C, O, P of FAR Part 25 and CS-25 of EASA.

Test methods for evaluating the performance characteristics of aircraft in in-flight icing conditions are flight tests in natural icing conditions, tests performed in simulated clouds produced by icing tankers and ground testing in icing wind tunnels. Flight testing is the most realistic way to observe the ice formation and the effects of icing on performance (Figure 1.1). However, it is expensive and time consuming since the actual atmospheric icing conditions, especially the extreme conditions for certification purposes are rare. Moreover, there exists safety issue, since the aerodynamic performance, controllability and data gathering under icing conditions are not certified and not fully perceived yet.



Figure 1.1. In-flight icing tests [17]

Another method for in-flight icing testing is testing in simulated clouds produced by icing tankers (Figure 1.2). This method permits the selection of icing parameters. Nonetheless, it is also expensive, the conditions are limited by tanker operational

limitations and other atmospheric parameters that affect icing cannot be controlled. In addition, it is not straightforward to keep two air vehicles in steady flight to ensure suitable test conditions.



Figure 1.2. Icing tests in simulated clouds produced by icing tanker [9]

The last testing method is testing in icing wind tunnels (Figure 1.3). Icing wind tunnels can provide natural icing conditions by cooling the water and obtain the droplets in the air by spraying. In icing wind tunnels, the cloud conditions, temperature, airspeed can be controlled, providing a safer and relatively inexpensive testing option. Thus, icing wind tunnel testing is the most convenient method considering feasibility, cost and safety.



Figure 1.3. Ice accretion on a wing in an icing wind tunnel [18]

In icing wind tunnels, the ice shapes are recorded for desired icing conditions. Knowing the ice shape for related simulated flight and cloud conditions, aerodynamic performance penalty can be obtained in flight or in aerodynamic wind tunnel by performing tests with addition of final known ice shape produced from a suitable material by a suitable method such as 3-D printing.

Although icing wind tunnel testing is convenient and preferable, there are some limitations regarding the icing wind tunnel operational capabilities. The test-section size and aerodynamic blockage constitute limitation of size of the test item. Furthermore, while simulating the natural icing conditions, icing wind tunnels have limited ranges of air speed, cloud droplet size and liquid water content (LWC). When the test model does not fit into the test-section, or the desired test conditions are outside the operational capabilities of the facility, a method that provides scaled ice accretions as the reference condition that is applicable for various icing conditions is required. Moreover, even though a validated scaling method is employed for scaling

for icing wind tunnel tests, validation for the specific test item and conditions must be performed before the icing wind tunnel testing for reliability and validity of the tests. The validation of the scaling method can be performed utilizing the computational tools available.

1.2. Literature Survey

In the past studies, different methods are utilized to obtain a scaled ice shape matching the reference ice shape. The similitudes that are mentioned in the literature regarding the icing scaling analysis are similitude of geometry, flow field, droplet trajectory, water catch, energy balance and surface water dynamics. The similitudes of the former are satisfied by deriving scaling parameters regarding each of the similitudes and matching them for scaled and reference cases. However, defining the scaling parameters and deciding their weight and importance have been a challenge through the years. Thus, according to the similitudes that are decided to be satisfied, different icing scaling parameters were suggested and various combinations of these parameters were employed as scaling methods to obtain similar ice accretions. Similitude of droplet trajectory is associated with modified inertia parameter, K_0 ; similitude of water catch is associated with accumulation parameter, A_c ; energy balance is associated with freezing fraction at stagnation, n_0 , relative heat factor, b , droplet energy transfer parameter ϕ , air energy transfer parameter, θ , and similitude of surface water dynamics is associated with We_L .

In the study presented by Hauger et al. which was conducted in Douglas Aircraft Company [15], the scaling method was suggested to be a combination of similitudes of droplet trajectory, water catch; which requires matching scaling parameters K_0 and A_c .

In the study presented by Sibley et al. which was conducted in Lockheed Aircraft Corporation [35], the scaling method was suggested to be a combination of similitudes of droplet trajectory, water catch and energy balance; so that, the scaling parameters to be matched was suggested as K_0 , A_c , n_0 and b .

In the study presented by Dodson which was conducted in Boeing Airplane Company [9], the scaling method was suggested to be a combination of similitudes of droplet trajectory, water catch that leads the scaling parameters sufficient for icing scaling are to be K_0 and A_c .

In the study presented by Jackson which was conducted in British Aircraft Corporation [20], the scaling method was suggested to be a combination of similitudes of droplet trajectory, water catch and energy balance. The scaling parameters were suggested as K_0 , A_c , n_0 and b , accordingly.

In the study presented by Armand et al. which was conducted in ONERA [5], the scaling method was suggested to be a combination of similitudes of droplet trajectory, water catch and energy balance. The scaling parameters to be matched for a scaling method to be effective was stated as K_0 , A_c , n_0 , b , ϕ and θ . For this method, extra importance is given to the energy balance by choosing all four of the energy balance similitude parameters (n_0 , b , ϕ and θ).

In the study presented by Ruff [34], a scaling method is developed by identifying the scaling parameters via investigation of equations governing icing process and performing tests in Arnold Engineering Development Center (AEDC) Engine Test Facility (ETF). The tests for verification of the scaling method were performed with full-scale and 1/2-scale cylinders and full-scale, 1/3-scale, 1/6-scale airfoil sections. The ice shapes obtained for scaled cases are compared with the full-scale results, so that the accuracy of the scaling method is verified. The scaling types are stated as size-scaling, icing condition scaling and the similitude is investigated via ensuring similitude of the flow field, the droplet trajectory and characteristics of impingement, the total amount of water impinging, and the thermodynamics of the ice accretion process. Some scaling methods were suggested that are combinations of similitudes of droplet trajectory, water catch and energy balance. And the energy balance similitude is ensured by different combinations of energy balance parameters which are n_0 , b , ϕ and θ . Some scaling methods are proposed such as, K_0 and A_c constant;

K_0 , A_c and n_0 constant; K_0 , A_c , n_0 and b constant and K_0 , A_c , n_0 , ϕ and θ constant. The final method is found to be the most accurate to obtain scaled ice shapes. The limitation of the scaling method is stated as the velocity because velocities that result in Reynolds number less than 2.0×10^5 and above critical Mach number have special characteristics that scaling is not straightforward. Moreover, a method for scaling water shedding is suggested but not verified completely which states around 1.6 psia dynamic pressure the shedding characteristics affect the final ice shape; thus, ice accretions do not match adequately when $q > 1.6$ psia.

In the study presented by Anderson [1], a scaling method is developed by identifying the scaling parameter by investigating icing and similitude physics and combining the knowledge of previous studies on icing scaling methods. The similitude is ensured by providing the similarity of geometry, flow field, droplet trajectory, water catch, energy balance and surface-water dynamics. Similarity parameters employed for size-scaling and test-condition scaling are described, and the effect of scaling parameters on final scaled ice shape and the physical phenomena constituting the icing parameters were interpreted performing tests at NASA Glenn Icing Research Tunnel. The Ruff method modified by constant We_L approach is recommended to calculate scale velocity and for obtaining reference ice shape with a scaled size model which is the method employed in current study. This method requires to match the droplet trajectory, water catch, energy balance and surface water dynamics in addition model non-dimensional geometry and angle of attack. The scaling parameters to be matched are selected as K_0 , A_c , n_0 , ϕ , θ and We_L for tunnels with altitude capability or K_0 , A_c , n_0 , We_L and one of the parameters ϕ , θ for sea-level tunnels. At this study, the most important novelty for scaling method is the addition of the effect of surface water dynamics that is included into the scaling method by the requirement matching of We_L . The We_L parameter drives the selection of scale velocity. The author states the practical limitations of size scaling due to both physical constrains and facility limitations, scale ratio smaller than $\frac{1}{2}$ to $\frac{1}{4}$ is not feasible for effective scaling and noted that there are limitations for test condition scaling as well but those limits are not investigated

sufficiently to make final conclusions. For future studies, a scaling method that includes 3-D effects was addressed. Studies on scaling for applications such as swept wings, rotorcraft and scaling for ice-protection systems were recommended.

In the study presented by Han et al. [14], ice accretion tests of a model wind turbine blade was performed in The Adverse Environment Rotor Test Stand (AERTS) at the V/STOL Research Center of Excellence. The modified Ruff method is employed for scaling a matrix of conditions for rime and glaze ice. The effect of angle of attack was found out to be small for small values of AOA ($2^\circ, 4^\circ$); however, for larger AOA values ($4^\circ, 8^\circ$), the effect was significant. The author stated that the effect of temperature is not effective for rime ice whereas it is effective for glaze ice cases.

1.3. Objectives

Objective of this study is to employ a scaling method that produces the same ice accretions for scaled conditions as the reference conditions and to validate the method before the icing wind tunnel tests with numerical analysis. A scaling method for size and test-condition scaling that is based on similitudes of geometry, flow field, droplet trajectory, water catch, energy balance and surface water dynamics is employed for scaling by Ruff and Duesterhaus in [34] and Anderson in [1]. Scaling method that is employed has scaling parameters that are K_0 , A_c , n_0 , We_L and one of the parameters ϕ , θ to match when the tunnel has constant total pressure. In current study, constant tunnel total pressure of 100 kPa is assumed and ϕ is selected as fifth scaling parameter.

The scaling method is implemented on icing cases in reference [37] and [1]. The ice accretions on airfoils NACA0012 and SA13112 are obtained for reference and scaled conditions with computational analyses using an in-house icing code AEROMSICE-2D and a commercial CFD tool ANSYS® Fluent 18.0 and in-flight icing code FENSAP-ICE. The ice accretions obtained by analyses are verified with experimental data in the literature [37] and the scaling method is tested for geometry scaling and velocity scaling at several Appendix-C icing conditions.

CHAPTER 2

IN-FLIGHT ICING PHYSICS

2.1. Ice Formation

Icing is one of the most dangerous hazards to be encountered in flight. Ice formation occurs when an air vehicle flies through super-cooled clouds. Super-cooled clouds contain super-cooled droplets which are droplets exist in liquid phase at temperatures below 0°C. Super-cooled droplets may freeze when they impact surfaces, creating an ice layer on the surface. Thus, ice may accrete on exposed frontal surfaces of an air vehicle. Ice accretions occur when ambient temperature is below 0°C and super-cooled droplets are present. There are two main ice types depending on the environmental icing conditions.

Rime ice that is shown in Figure 2.1 representatively, occurs at low ambient temperatures and low LWC. Cloud droplets may freeze instantaneously in contact with the surface and form rime ice. Rime ice is opaque and usually follows the surface contour. It is easier to detect and remove.

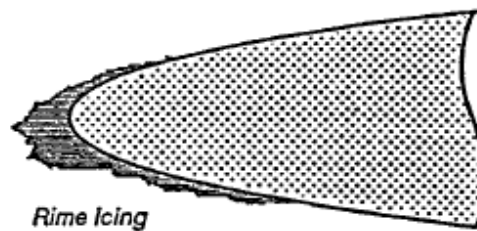


Figure 2.1. Rime ice [30]

Glaze (clear) ice that is shown in Figure 2.2 representatively, occurs at relatively higher ambient temperatures (around freezing temperature) and higher LWC. A fraction of droplets freezes on impact; remaining droplets may flow downstream on surface that is defined as runback water. Runback water may freeze downstream forming runback ice. Glaze ice is transparent, forms in irregular shapes. It is hard to detect and remove.

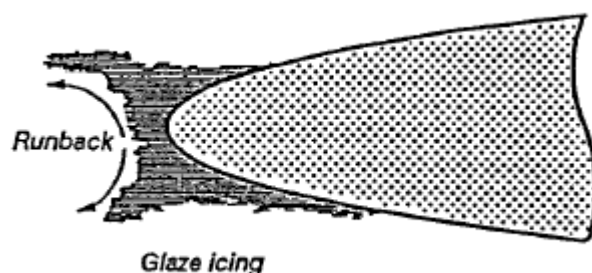


Figure 2.2. Glaze (clear) ice [30]

2.2. Factors Affecting Icing

The ice accretion amount and shape depend on a number of meteorological and aerodynamic conditions including liquid water content (LWC), droplet size, and temperature, and airspeed, size of the object and exposure time. Water catch and collection efficiency are factors affecting ice accretion. Water catch is amount of water that impinges the surface and depends on the LWC, airspeed and exposure time. Collection efficiency is defined as the ratio of the mass of droplets impinges on a body in unit time to the mass of droplets that would impinge if the droplets were following straight line trajectories that is illustrated in Figure 2.3.

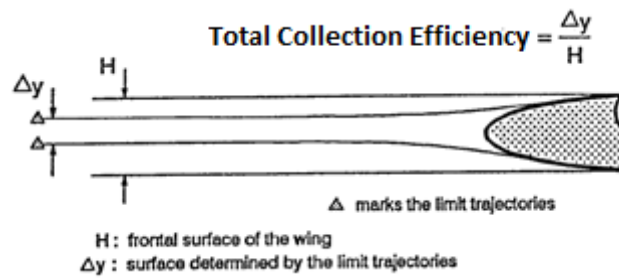


Figure 2.3. Total collection efficiencies [30]

2.2.1. Liquid Water Content (LWC)

Liquid water content (LWC) is the ratio of water mass present in a unit volume of dry air. The values of LWC are measured for different cloud types and exposure times with flight tests given in FAR/CS 25 Appendix C [22]. LWC indicates the severity of icing, type and shape of ice that forms. As LWC increases and other parameters affecting icing remain constant, the ice accretion increases (Figure 2.4).

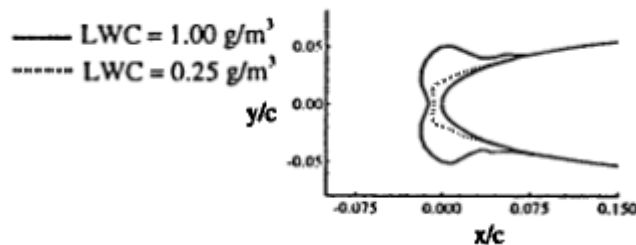


Figure 2.4. Effect LWC on ice accretion [30]

2.2.2. Droplet Size

Droplet size also expressed as median volumetric diameter (MVD), determines the type and rate of icing through the droplet collection efficiency. Increasing droplet size increases kinetic energy of incoming droplets that leads to more impingement; thus, as droplet size increases, collection efficiency increases (Figure 2.5 and Figure 2.6).

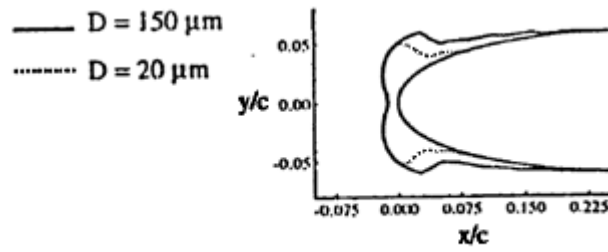


Figure 2.5. Effect of droplet size on ice accretion [30]

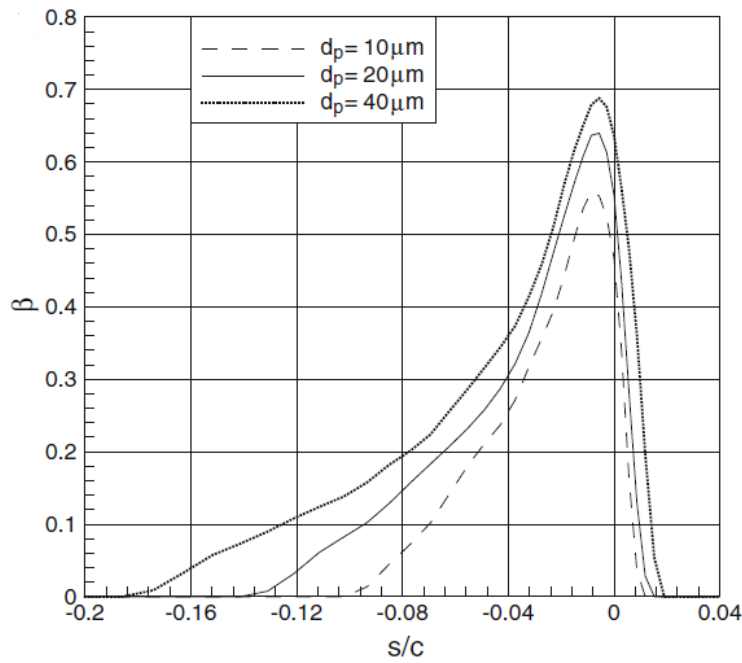


Figure 2.6. Effect of droplet size on collection efficiency [27]

2.2.3. Temperature

Ambient temperature has an effect on the type and intensity of ice. The characteristic of ice that is forming is directly related to the temperature (Figure 2.7).

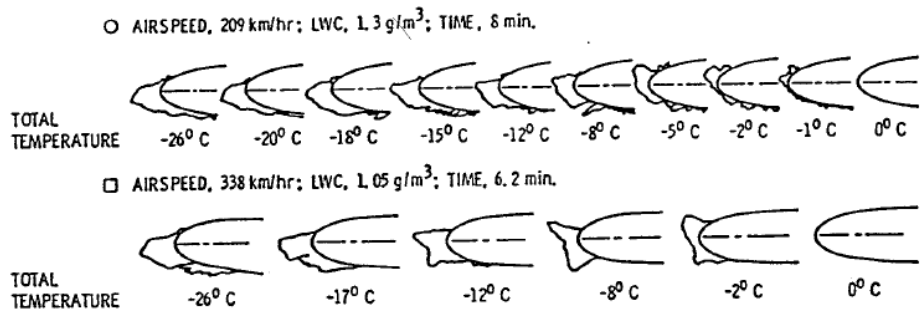


Figure 2.7. Effect of total temperature on ice accretion [30]

2.2.4. Size of the Object

Larger objects create more deviation for the incoming droplets, causing less impingement that leads to a decrease in collection efficiency (Figure 2.8).

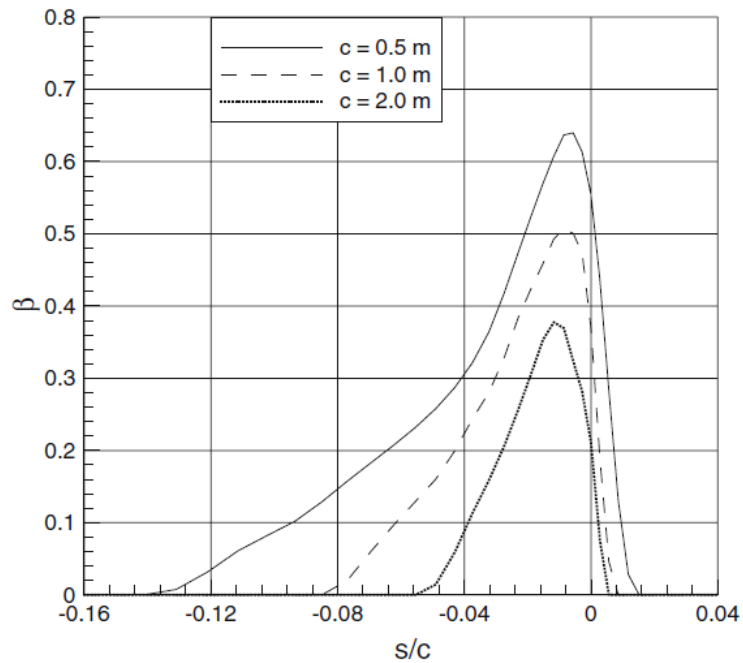


Figure 2.8. Effect of airframe size on collection efficiency [27]

2.2.5. Airspeed

Increasing airspeed increases kinetic energy of incoming droplets that leads to more impingement; thus, as airspeed increases, collection efficiency increases. Increased collection efficiency results in increased ice accretion (Figure 2.9). However, increasing airspeed also increases aerodynamic heating that increases surface temperature and may reduce ice accretion.

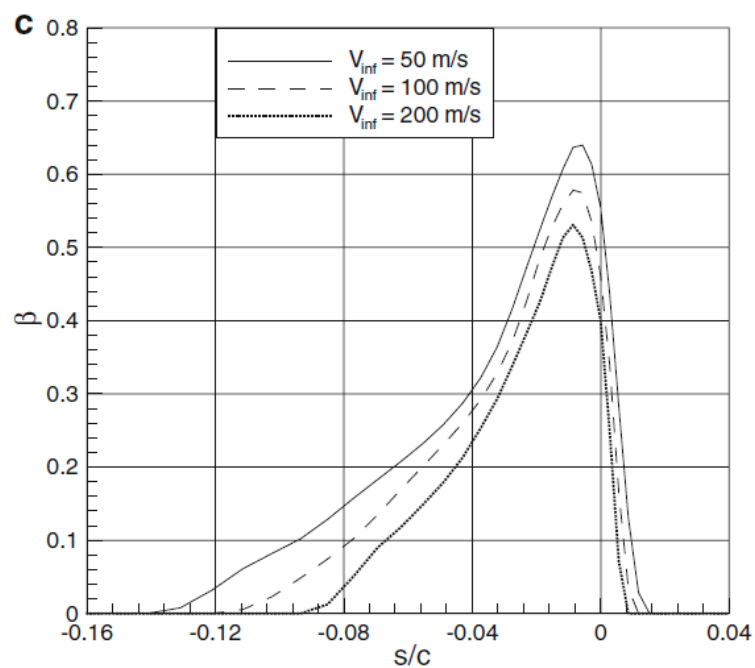


Figure 2.9. Effect of airspeed on collection efficiency [27]

2.2.6. Exposure Time

Exposure time increases the amount of ice accretion since the total amount of droplets impinging on the surface increases with time.

CHAPTER 3

ICING PREDICTION

The icing prediction is performed computationally by in-house icing code AEROMSICE-2D and a CFD tool ANSYS® Fluent 18.0 and in-flight icing code FENSAP-ICE and presented in this chapter.

AEROMSICE-2D is an in-house code that solves 2-D flow field, droplet trajectories and ice accretion that is developed and published by Özgen and Canıbek in [28].

The parts of calculations consist of flow field solution, droplet trajectories and collection efficiencies, thermodynamic analysis and ice accretion modeling.

3.1. Flow Field Solution

The flow field solution is required for obtaining velocity and pressure distributions on the geometry to be input to boundary layer and droplet trajectory calculations.

3.1.1. AEROMSICE-2D

The in-house code employs Hess-Smith panel method [23] coupled with a boundary-layer solver.

The airfoil is divided into N line segments that are referred as panels. Each panel is associated with a source and vortex singularity element. Source singularity strength is constant for each panel and vortex singularity strength is constant for all panels. The N source and one vortex singularity strengths are the $N+1$ unknowns. The strengths are solved using flow tangency boundary condition at the collocation points of the panels that are their centroids. The Kutta-condition introduces a new equation to the system.

With singularity strengths known, velocity potential can be constructed and velocity components of the air flow at any location in the flow field can be calculated including

the boundaries of the airfoil. In addition, convective heat transfer distribution around the airfoil is calculated by integral boundary layer method employing the inviscid velocity distribution obtained by panel method.

3.1.2. FENSAP-ICE

The flow field is solved by commercial software ANSYS® Fluent 18.0 and provided to the in-flight icing code FENSAP-ICE. The flow field solution is obtained by solving Reynolds Averaged Navier Stokes Equations by a finite volume method (FVM) for the spatial discretization. Turbulence is modeled with two equation $k-\omega$ SST turbulence model.

Navier-Stokes Equations describe the relation between velocity, pressure, temperature, and density of the flow. The Navier-Stokes equations are Euler Equations with addition of viscosity effects on the flow. The equations are a set of coupled differential equations consists of a continuity equation for conservation of mass, two conservation of momentum equations and a conservation of energy equation. The unknowns are pressure, density, and temperature that are coming from energy equation and velocity vector components. To solve the system of equations, an additional equation is required that relates the pressure, temperature, and density of the air, that is equation of state.

Theoretically the equations can be solved analytically, however, in reality due to its complexity, methods like finite difference, finite volume, finite element are employed to solve the equations approximately, that refers to the Computational Fluid Dynamics or CFD.

For turbulent flows, velocity fluctuations and turbulent phenomena further increase the complexity of the problem. Thus, instead of calculating turbulent quantities, modeling the turbulent behavior has become a widely accepted method.

To be able to model the turbulence, the solution variables in Navier-Stokes equations divided into mean (time averaged) and fluctuating components. The new forms of the

variables are substituted into continuity and momentum equations and the equation is time-averaged to avoid simulating all scales of the turbulence spectrum yielding Reynolds-averaged Navier-Stokes (RANS) equations. Even though the general form of RANS equations is the same as the exact Navier-Stokes equations, the variables now represent time averaged values and some additional terms are present due to turbulence effects. The additional terms are Reynolds stresses are modeled by Boussinesq hypothesis that relates the Reynolds stresses to the mean velocity gradients by a isotropic turbulent viscosity, μ_t , [16].

There are several turbulence models that model the Reynolds stresses by turbulent viscosity. For this study, the two-equation SST k - ω turbulence model is selected. The SST k - ω turbulence model turbulent viscosity is modeled as a function of turbulence kinetic energy, k , and the specific dissipation rate, ω . The model computes turbulent viscosity by adding two additional transport equations for k , and ω to RANS equations. The model combines effectively the robust and accurate formulation of the k - ω model in the near-wall region with the free stream independence of the k - ϵ model in the far field [24], [4].

3.2. Droplet Trajectories and Collection Efficiencies

3.2.1. AEROMSICE-2D

Droplet trajectories are calculated utilizing Lagrangian approach with the assumptions that are valid for droplet sizes below 500 μm that includes the range for this study:

- Droplets are spherical.
- Droplets have no effect on the flow field.
- The only forces acting on the droplets are gravity and aerodynamic drag.
- Heat and mass transfer (evaporation) between the droplet and flow are neglected.
- The droplets are at the same temperature as the flow.

The governing equations for 2-D droplet trajectories are as follows:

$$m\ddot{x}_d = -D \cos \gamma \quad (1)$$

$$m\ddot{y}_d = -D \sin \gamma + mg \quad (2)$$

$$\gamma = \tan^{-1} \frac{\dot{y}_d - V_y}{\dot{x}_d - V_x} \quad (3)$$

$$D = \frac{1}{2} \rho_a V_{rel}^2 C_D A_d \quad (4)$$

$$V_{rel} = \sqrt{(\dot{x}_d - V_x)^2 + (\dot{y}_d - V_y)^2} \quad (5)$$

where V_x, V_y are components of flow velocity, $\dot{x}_d, \dot{y}_d, \ddot{x}_d, \ddot{y}_d$ are droplet velocity and acceleration components, respectively. A_d denotes droplet cross sectional area and C_D is droplet drag coefficient [12].

The drag coefficients of the droplets are calculated from [12]:

$$C_D = \frac{24}{Re_d} (1 + 0.197 Re_d^{0.63} + 2.6 \times 10^{-4} Re_d^{1.38}) \quad Re_d \leq 3500 \quad (6)$$

$$C_D = \frac{24}{Re_d} (1.699 \times 10^{-5}) Re_d^{1.92} \quad Re_d > 3500 \quad (7)$$

Reynolds number based on droplet diameter d_d and relative velocity of droplets with respect to free stream V_{rel} and the viscosity μ is calculated using Sutherland's law as a function of temperature:

$$Re_d = \frac{\rho_a V_{rel} \delta}{\mu} \quad (8)$$

Droplet trajectories are obtained by integrating equations 1 and 2 with respect to time from an upstream location sufficiently far from the airfoil, until droplet reaches the airfoil either impacting or missing the surface. At upstream, the release plane of the droplets, the velocity of the droplets are taken as terminal velocity given in equation 9.

$$V_{term}^2 = \frac{4}{3} \frac{(\rho_w - \rho_a) g \delta}{\rho C_D} \quad (9)$$

The impingement limits and water mass on the airfoil is determined by the droplet distribution obtained by trajectory analysis. The local collection efficiency is defined as the droplet impingement area on the airfoil to the area of impinging droplets constitutes on the release plane (Figure 3.1). The two-dimensional local collection efficiency formulation is:

$$\beta = \frac{\Delta y_0}{\Delta s} \quad (10)$$

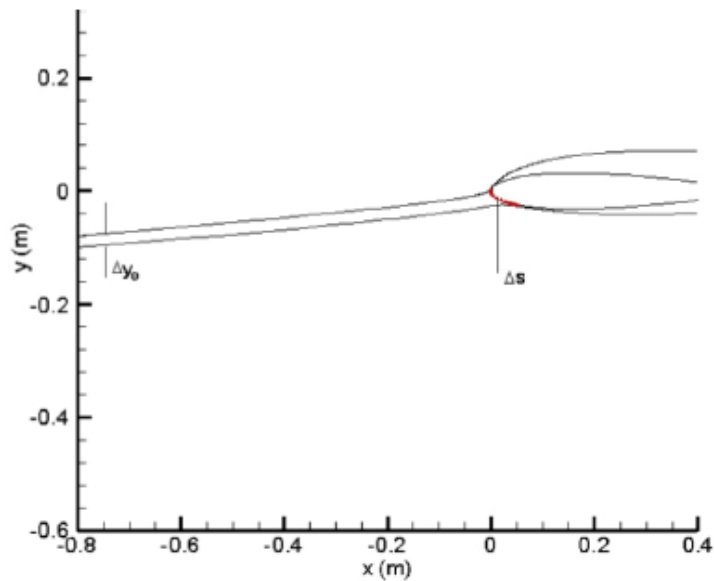


Figure 3.1. Definition of collection efficiency [28]

3.2.2. FENSAP-ICE

Droplet trajectories are calculated in DROP3D module utilizing Eulerian two-fluid model that is Navier-Stokes equations with the addition of droplets to the continuity and momentum equations. The velocity of droplets and liquid water content are introduced to the freestream. Droplet velocity is zero on the walls for the initial iteration. The FEM is used to discretize the equations, with addition of a streamline unwinding Petrov–Galerkin stabilization term [17].

The LWC and droplet velocity are computed at the nodes the nodes where the airflow variables are known from flow solution Thus, no particle tracking is performed for droplet trajectories like Lagrangian approach.

The assumptions are as follows [8]:

- The droplets are spherical (no deformation or breaking);
- Droplets collision, coalescence or splashing are neglected;

- Heat and mass transfer between the droplets and the air is neglected;
- Turbulence effects on the droplets are neglected;
- The only forces acting on the droplets are drag, gravity and buoyancy.

The first two assumptions are applicable for icing droplets since they are small (1-100 microns range) and the volume fraction of icing droplets in air should be around 10^{-6} .

Navier–Stokes equations for dry air with water volume fraction-related continuity and momentum equations [27]:

$$\frac{\partial \alpha}{\partial t} + \nabla \cdot (\alpha \mathbf{V}_d) = 0 \quad (11)$$

$$\frac{\partial (\alpha \mathbf{V}_d)}{\partial t} + \nabla \cdot (\alpha \mathbf{V}_d \mathbf{V}_d) = \frac{C_D \text{Re}_d}{24K} \alpha (\mathbf{V}_a - \mathbf{V}_d) + \alpha \left(1 - \frac{\rho_a}{\rho_d}\right) \frac{1}{Fr^2} \quad (12)$$

where, α is water volume fraction, V_a , V_d are air and droplet velocity, respectively. Re_d is droplet Reynolds number and Fr is Froud number.

An inertial parameter:

$$K = \frac{\rho_d V_\infty \delta^2}{18L\mu} \quad (13)$$

Local Froud number:

$$Fr = \frac{V_\infty}{\sqrt{Lg}} \quad (14)$$

Drag coefficient for droplets is calculated with an empirical correlation for flow around spherical droplets that is valid for droplet sizes below $250 \mu\text{m}$ that includes the range for this study:

$$C_D = \frac{24}{Re_d} (1 + 0.15Re_d^{0.687}) \quad Re_d \leq 1300 \quad (15)$$

$$C_D = 0.4 \quad Re_d > 1300 \quad (16)$$

The Eulerian droplet trajectory equations are hyperbolic; thus, a boundary condition is needed. An initial solution is given by $\alpha = 1$ and $V = V_\infty$ everywhere but close to the airfoil surface, where both variables are set to zero. V_∞ may be a combination of the flow velocity at the far field, V_∞ and the droplets terminal velocity, V_{term} .

3.3. Thermodynamic Analysis

3.3.1. AEROMSICE-2D

To perform the thermodynamic analysis, convective heat transfer coefficient around the airfoil is required. Two-dimensional integral boundary layer method is utilized for calculation of convective heat transfer coefficients. Boundary-layer calculations start from the leading edge to the trailing edge for upper and lower surfaces of the airfoil. Transition is predicted from the roughness Reynolds number. According to Von Doenhoff criterion, transition occurs at $Re_k = 600$. Thus, transition location is where the roughness Reynolds number reaches this value.

Reynolds number based on roughness height:

$$Re_k = \frac{\rho_a V_k k_s}{\mu_a} \quad (17)$$

where k_s is the roughness height and V_k is the local flow velocity at the roughness location [31].

The flow velocity at the roughness location:

$$\frac{V_k}{V_e} = 2 \frac{k_s}{\delta} - 2 \left(\frac{k_s}{\delta} \right)^3 + \left(\frac{k_s}{\delta} \right)^4 + \frac{1}{6} \frac{\delta^2}{v} \frac{dV_e}{ds} \frac{k_s}{\delta} \left(1 - \frac{k_s}{\delta} \right)^3 \quad (18)$$

where V_e is flow velocity outside the boundary-layer at the roughness location.

The roughness height:

$$k_s = \frac{4\sigma_w\mu_w}{\rho_w F \tau} \quad (19)$$

where σ_w , ρ_w and μ_w denote the surface tension, density and viscosity of water, respectively. F is ratio of wetted airfoil area by droplets and τ is the local shear stress [37].

Laminar boundary layer thickness at $Re_k < 600$ [31]:

$$\delta = \frac{315}{37} \theta_l \quad (20)$$

where laminar momentum thickness by Thwaites formulation:

$$\frac{\theta_l^2}{v} = \frac{0.45}{V_e^6(s)} \int_0^s V_e^5(s) ds \quad (21)$$

In equation 21, s is streamwise distance along the airfoil surface starting at the stagnation point, v is dynamic viscosity of air.

The equation of Smith and Spalding is employed in order to calculate the convective heat transfer coefficient for laminar flow.

$$h_c = \frac{0.296kV_e^{1.435}}{\sqrt{v \int_0^s V_e^{1.87} ds}} \quad (22)$$

where k is the thermal conductivity of air.

Turbulent momentum thickness:

$$\theta_t = \frac{0.036v^2}{V_e^{3.29}} \left(\int_{s_{tr}}^s V_e^{3.86}(s) ds \right)^{0.8} + \theta_{tr} \quad (23)$$

where s_{tr} is transition location where $Re_k = 600$ and θ_{tr} is laminar momentum thickness at $s = s_{tr}$.

The equation of Kays and Crawford is employed in order to calculate the convective heat transfer coefficient for turbulent flow.

$$h_c = St\rho V_e C_p \quad (24)$$

where C_p is the specific heat of air and St is the Stanton number:

$$St = \frac{C_f/2}{Pr_t + \sqrt{(C_f/2)/St_k}} \quad (25)$$

where Pr_t is turbulent Prandtl number that is taken $Pr_t = 0.9$ and St_k is roughness Stanton number:

$$St_k = 1.92Re_k^{-0.45}Pr^{-0.8} \quad (26)$$

where laminar Prandtl number is taken as $Pr = 0.72$.

Turbulent skin friction coefficient from the Makkonen relation [12]:

$$\frac{C_f}{2} = \frac{0.1681}{\left[\ln \left(864 \frac{\theta_t}{k_s} + 2.568 \right) \right]^2} \quad (27)$$

The roughness height:

$$k_s = 0.00117 K_{V_\infty} K_{LWC} K_{T_a} K_{d_d} c \quad (28)$$

where K_{V_∞} , K_{LWC} , K_{T_a} and K_{d_d} are empirical factors accounting for freestream velocity, liquid water content, ambient temperature and droplet size effects, while c denotes the chord of the airfoil [37].

3.3.2. FENSAP-ICE

Frictional forces and heat fluxes from the viscous flow solution is provided by ANSYS® Fluent 18.0 flow solution.

For ice accretion calculations heat transfer coefficient is obtained from the convective heat transfer calculated by the flow solver [13], [4].

3.4. Ice Accretion Modeling

3.4.1. AEROMSICE-2D

Ice accretion on a surface is a phase change problem that is also referred as the Stefan problem. Extended Messinger Model is employed for the solution. The governing equations are energy equations for ice and water, mass balance equation and phase change at the ice-water interface [26].

$$\frac{\partial T}{\partial t} = \frac{k_i}{\rho_i C_{pi}} \frac{\partial^2 T}{\partial y^2} \quad (29)$$

$$\frac{\partial \theta_w}{\partial t} = \frac{k_w}{\rho_w C_{pw}} \frac{\partial^2 \theta_w}{\partial y^2} \quad (30)$$

$$\rho_i \frac{\partial B}{\partial t} + \rho_w \frac{\partial h}{\partial t} = LWC\beta V_\infty + \dot{m}_{in} - \dot{m}_{e,s} \quad (31)$$

$$\rho_i L_F \frac{\partial B}{\partial t} = k_i \frac{\partial T}{\partial y} - k_w \frac{\partial \theta_w}{\partial y} \quad (32)$$

The coordinate y is normal to the surface. θ_w and T are the temperature distributions, h and B are the thicknesses of water and ice layers, respectively. Ice density is assumed to have different values for rime ice, ρ_r and glaze ice, ρ_g .

The boundary and initial conditions for equations 29 to 32 based on the following assumptions [30]:

- Ice is in perfect contact with the airfoil:

$$T(0, t) = T_s \quad (33)$$

- The surface temperature is taken as the recovery temperature:

$$T_s = T_a + \frac{V_\infty^2 - V_e^2}{2C_p} \frac{1 + 0.2rM^2}{1 + 0.2M^2} \quad (34)$$

where $M = V_\infty/a_\infty$, and the speed of sound is given by $a_\infty = \sqrt{\gamma RT_a}$. Additionally, r is the adiabatic recovery factor ($r = Pr^{1/2}$ for laminar flow and $r = Pr^{1/3}$ for turbulent flow).

- The temperature is continuous at the ice-water contact and is equal to the freezing temperature, T_f :

$$T(B, t) = \theta_w(B, t) = T_f \quad (35)$$

- At air-ice interface for rime ice ($y = B$):

$$-k_i \frac{\partial T}{\partial y} = (Q_c + Q_s + Q_d + Q_r) - (Q_a + Q_k + Q_{in} + Q_i) \quad (36)$$

- At air-water interface for glaze ice ($y = B + h$):

$$-k_w \frac{\partial \theta_w}{\partial y} = (Q_c + Q_e + Q_d + Q_r) - (Q_a + Q_k + Q_{in}) \quad (37)$$

where, convection:

$$Q_c = h_c(T_s - T_a) \quad (38)$$

Cooling due to incoming droplets

$$Q_d = LWC\beta V_{\infty} C_{pw}(T_s - T_a) \quad (39)$$

Heat brought in by runback water:

$$Q_{in} = \dot{m}_{in} C_{pw}(T_f - T_s) \quad (40)$$

Evaporation

$$Q_e = \chi_e e_0(T_s - T_a) \quad (41)$$

Evaporation coefficient:

$$Q_e = \chi_e e_0(T_s - T_a) \quad (42)$$

where χ_e is the evaporation coefficient and $e_0 = 27.03$.

$$\chi_e = \frac{0.622 h_c L_E}{C_p P_t L_e^{2/3}} \quad (43)$$

Sublimation

$$Q_s = \chi_s e_0 (T_s - T_a) \quad (44)$$

Sublimation coefficient:

$$\chi_s = \frac{0.622 h_c L_S}{C_{pa} P_t L_e^{2/3}} \quad (45)$$

Aerodynamic heating

$$Q_a = \frac{r h_c V_\infty^2}{2 C_p} \quad (46)$$

Kinetic energy of incoming droplets

$$Q_k = \frac{LWC\beta V_\infty^3}{2} \quad (47)$$

Latent heat release

$$Q_k = \rho_r L_F \frac{\partial B}{\partial t} \quad (48)$$

Heat loss by radiation

$$Q_r = 4\epsilon\sigma_r T_a^3 (T_s - T_a) \quad (49)$$

- Surface is initially clean:

$$B = h = 0, \quad t = 0 \quad (50)$$

Rime ice growth:

$$B(t) = \frac{LWC\beta V_\infty + \dot{m}_{in} - \dot{m}_{e,s}}{\rho_r} t \quad (51)$$

Temperature distribution in the rime ice layer:

$$T(y) = T_s + \frac{(Q_a + Q_k + Q_{in} + Q_l) - (Q_c + Q_s + Q_d + Q_r)}{k_i} y \quad (52)$$

Glaze ice growth:

$$\rho_g L_f \frac{\partial B}{\partial t} = \frac{k_i(T_f - T_s)}{B} + k_w \frac{(Q_c + Q_e + Q_d + Q_r) - (Q_a + Q_k + Q_{in})}{k_w} \quad (53)$$

For the upper surface it is assumed that the water does not freeze, runs back to the neighboring downstream cell and for the lower surface all water sheds [11].

The glaze ice thickness is obtained by integrating equation 53 numerically by Runge-Kutta-Fehlberg method.

The temperature distribution in the ice layer:

$$T(y) = \frac{(T_f + T_s)}{B} + T_s \quad (54)$$

And the temperature distribution in the water layer is:

$$\theta_w(y) = T_f + \frac{(Q_a + Q_k + Q_{in}) - (Q_c + Q_e + Q_d + Q_r)}{k_w} (y - B) \quad (55)$$

Water layer thickness for glaze ice:

$$B_g = \frac{k_i(T_f - T_s)}{(LWC\beta V_\infty + \dot{m}_{in} - \dot{m}_s)L_F + (Q_a + Q_k + Q_{in}) - (Q_c + Q_e + Q_d)} \quad (56)$$

where B_g is the rime ice thickness at which glaze ice first forms, and t_g is the corresponding time:

$$t_g = \frac{\rho_r}{(LWC\beta V_\infty + \dot{m}_{in} - \dot{m}_s)} B_g \quad (57)$$

3.4.2. FENSAP-ICE

Ice accretion computations in FENSAP-ICE software are performed in ICE3D module. The frictional forces and heat fluxes are imported from the viscous flow solution provided by ANSYS® Fluent 18.0 and the water volume fraction provided by DROP3D. Ice accretion is modeled by modifying classical Messinger model into partial differential equations [25],[7]. The Figure 3.2 represents the module interactions in FENSAP-ICE software as a flowchart.

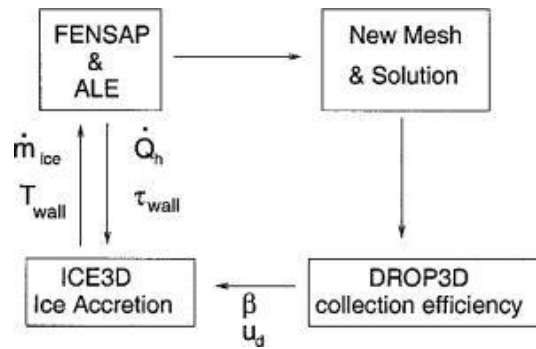


Figure 3.2. Module interactions in FENSAP-ICE [5]

The Figure 3.3 shows the heat and mass transfer scheme that is modeled for ice accretion. On the surface the droplet impingements are modeled as thin film. The film may flow downstream as runback, completely or partially freeze (rime or glaze ice accretion), evaporate or sublimate.

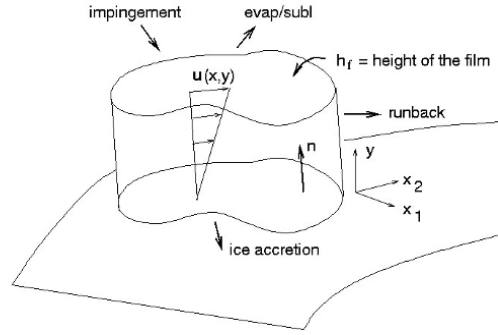


Figure 3.3. Ice accretion in ICE-3D [2]

The model predicts no liquid water when the equilibrium temperature is below freezing temperature and no ice formation occurs when the film temperature is above freezing temperature. However, ice can still accumulate when surface temperature is above freezing temperature due to cooling by evaporation.

The velocity of water in the film layer on the surface is $V_{film}(x, y)$ and it is a function of spatial coordinates, x on the surface and y normal to the surface. The terms of order higher than one in the velocity profile are negligible for very thin films, and the film thickness is usually below 10 microns [36].

Assuming linear profile for velocity, and zero initial velocity at surface:

$$V_{film}(x, y) = \left(\frac{\tau_s}{\mu_w} - \frac{h}{\mu_w} \frac{dp}{ds} \right) y(x) \quad (58)$$

where h is the water film thickness, τ_s is the shear stress on the surface due to air flow which is the dominant force on water film. The pressure force is negligible except near the stagnation point.

The 2-D dimensionless pressure gradient at stagnation point [33]:

$$-\frac{s}{\rho V_e^2} \frac{dp}{ds} = 1 \quad (59)$$

where V_e is the velocity just outside of the boundary layer and s is the distance from stagnation point.

Pressure forces are negligible in the condition:

$$\tau_s \gg h \frac{dp}{ds} \quad (60)$$

When friction coefficient definition and equation 59 are utilize to obtain a new form for equation 60:

$$0.5C_f \gg \frac{h}{s} \quad (61)$$

Thus, for small film thickness h , the pressure gradient has an effect near a stagnation point or a separation point [21].

Mean velocity formulation by the average along the film thickness is:

$$\bar{V}_{film}(x, y) = \frac{1}{h} \int_0^h V_{film}(x, y) dy = \frac{h}{2\mu_w} \tau_s(x) \quad (62)$$

Since the water film is very thin, in the direction normal to the wall temperature change is small. Thus, along the water film a constant average temperature is taken.

The partial differential equation system is:

Conservation of mass:

$$\rho_w \left(\frac{\partial h}{\partial t} + \nabla \cdot (\bar{V}_{film} h) \right) = LWC\beta V_\infty - \dot{m}_e - \dot{m}_i \quad (63)$$

The right-hand side consists of mass coming from impinging water droplets, the evaporation and ice accretion, respectively. T is the surface temperature.

Conservation of energy:

$$\begin{aligned} \rho_w \left(\frac{\partial h C_{pw} T_{film}}{\partial t} + \nabla \cdot (\bar{V}_{film} h C_{pw} T_{film}) \right) & \quad (64) \\ & = \left(C_{pw} T_d + \frac{V_d^2}{2} \right) LWC\beta V_\infty - 0.5(L_E + L_S)\dot{m}_e \\ & + (L_F - C_{pi} T_{film})\dot{m}_i + \epsilon\sigma(T_\infty^4 - T_{film}^4) + \dot{Q}_c \end{aligned}$$

The right-hand side consists of heat transfer due to impinging droplets, evaporation, ice accretion, radiation and convection, respectively.

It is assumed that half of the water is considered liquid and half of the water is solid when evaporation is in progress [21]. Conduction through the airfoil skin is neglected since the ice acts like an insulator [38].

The heat transfer coefficients are obtained from convective heat transfer coefficient provided by the flow solver.

$$h_c = \frac{\dot{Q}_c}{(T_{film} - T_\infty)} \quad (65)$$

The heat transfer coefficient is strongly dependent on boundary layer thickness and weakly dependent on the surface temperature distribution on the airfoil. Thus, for the

calculations a fixed $h_c(x)$ is taken as an input to equation 65 to obtain convective heat flux that depends on the surface temperature.

T_d , V_∞ , LWC , and T_∞ , are air and droplet parameters that are user inputs.

Local collection efficiencies β and droplet impact velocities V_d are provided by the Eulerian droplet module DROP3D. The local wall shear stress τ_s and the convective heat flux \dot{Q}_c are provided by the flow solver ANSYS® Fluent 18.0. The evaporative mass flux is recovered by a parametric model [38].

Remaining three unknowns the film thickness h , the equilibrium temperature between air-water film-ice-wall T_{film} and the mass accumulation of ice \dot{m}_i . Following relations are utilized to close the system:

$$h \geq 0 \quad (66)$$

$$\dot{m}_i \geq 0 \quad (67)$$

$$hT_{film} \geq 0 \quad (68)$$

$$\dot{m}_iT_{film} \leq 0 \quad (69)$$

Finite volume method is employed for the discretization. The surface mesh is defined as air-structure/ice shape interface. From surface mesh by connecting the mid-edges of cells to the centroids of the cells a dual surface mesh is obtained (Figure 3.4). The unknowns are computed at the center of each dual cell corresponding one-to-one to the nodes of the FEM used for the air and droplet solutions.

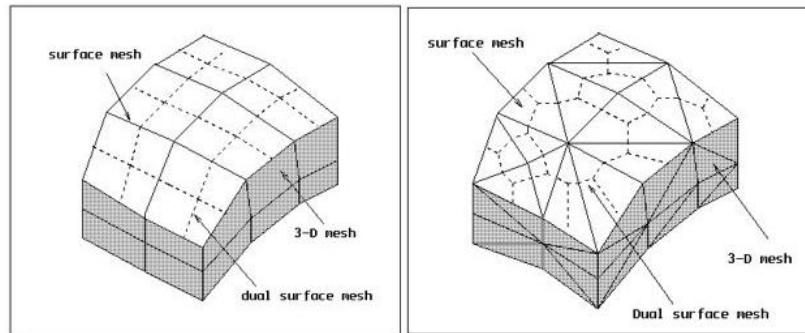


Figure 3.4. Ice accretion in ICE-3D [2]

As the ice accretion solution is obtained, ice accretion solver gives wall temperature distribution and the displacements of the surface nodes. These are input to the airflow solution and start a new calculation cycle.

CHAPTER 4

ICING SIMILITUDE ANALYSIS

For in flight icing to occur, supercooled droplets must be present and ambient temperature must be below 0°C . Droplets may freeze instantaneously after impingement and form rime ice or some of the impinging droplets may freeze and some may run downstream and freeze later forming glaze ice. The freezing fraction is the ratio of the amount of water that freezes at impingement to the total amount of impinging water. Thus, the freezing fraction is unity for rime ice and it takes a value between 0 and 1 for glaze ice. The icing type changes the characteristics of ice formation and final ice shape. Rime ice is a dry, opaque ice which usually forms at low airspeed, low temperatures and low liquid water content icing environments, while glaze ice is a wet ice which forms at temperatures around 0°C , and high liquid water content icing environments.

A scaling method that produces similar ice accretions for scaled model size and/or test conditions requires the similitudes of geometry, flow field, droplet trajectory, water catch, energy balance and surface water dynamics [34],[1]. For rime ice, since all supercooled droplets that contact the surface freeze immediately and there is no water film layer, achieving energy balance and surface water dynamics similitudes is not necessary, first four similitudes are enough to achieve ice accretion similarity for rime ice.

4.1. Geometric similarity

The shape and material of scaled geometry and reference geometry should be similar for similar flow and icing physics.

4.2. Flow field similarity

Flight condition similitude is achieved by matching the Mach number and Reynolds Number for reference and scaled conditions. Where static temperature and pressure are determined by the icing condition, $\gamma = 1.4$ and $R_a = 287.05 \text{ J/kg K}$.

$$M = \frac{V}{\sqrt{\gamma R_a T}} \quad (70)$$

$$Re_a = \frac{V L \rho_a}{\mu_a} \quad (71)$$

Reference length L is taken as the airfoil leading edge radius. Air density and viscosity are calculated as follows:

$$\rho_a = \frac{P_{st}}{R_a T_{st}} \quad (72)$$

$$\mu_a = \frac{10^{-4}}{0.12764 + 124.38 \left(\frac{K}{T_{st}} \right)} \frac{g}{cm \ s} \quad (73)$$

However, matching these simultaneously is not feasible considering that the parameters constituting these numbers also constitute more critical scaling parameters regarding the droplet trajectory and ice accretion. Thus, for most scaling analyses matching the Mach number and Reynolds Number is not aimed. This assumption might be justified considering the fact that in majority of the icing conditions, the Mach number is relatively low and compressibility effects are negligible and ice accretion occurs near the stagnation regions, where the boundary layer is thin and viscous effects are rather small.

Therefore, the similarity of flow field is considered to be achieved when the Mach number and Reynolds number is in the interval of $M_{Re=2 \times 10^5} < M < M_{critical}$ near the stagnation region, [34]. Lower limit corresponds to a Reynolds number that the velocity distribution is preserved up to stall and upper limit corresponds to critical Mach number where the supersonic flow is first seen on the geometry.

4.3. Droplet trajectory similarity

Droplet impingement zones and droplet trajectories should be matched for droplet trajectory similitude. Modified inertia parameter, K_0 , and collection efficiency, β_0 , should be matched for droplet trajectory similarity.

$$K_{0,S} = K_{0,R} \quad (74)$$

$$K_0 = \frac{1}{8} + \frac{\lambda}{\lambda_{Stokes}} \left(K - \frac{1}{8} \right) \quad (75)$$

$$K = \frac{\rho_w \delta^2 V}{18 L \mu_a} \quad (76)$$

where $\rho_w = 1g/cm^3$.

$$\frac{\lambda}{\lambda_{Stokes}} = \frac{1}{0.8388 + 0.001483 Re_\delta + 0.1847 \sqrt{Re_\delta}} \quad (77)$$

$$Re_\delta = \frac{V \delta \rho_a}{\mu_a} \quad (78)$$

4.4. Water catch similarity

$$\beta_0 = \frac{1.40 \left(K_0 - \frac{1}{8}\right)^{0.84}}{1 + 1.40 \left(K_0 - \frac{1}{8}\right)^{0.84}} \quad (79)$$

The amount of ice accreted depends on the amount of water that impinges the surface. For ice accretion similitude, water catch parameters should match.

$$A_{c,S} = A_{c,R} \quad (80)$$

$$A_c = \frac{LWC V t_{exp}}{\rho_i L} \quad (81)$$

where $\rho_i = 0.917 \text{ g/cm}^3$.

4.5. Energy balance similarity

Ice accretion occurs when the supercooled droplets hit the air vehicle surface and freezes immediately or a fraction of them freezes and remainder freeze downstream. For the first case, that is the formation of rime ice, there is no need for energy balance similitude since all impinging water freezes at the instant of impingement, at impinging point.

Ice accretes near stagnation point. Thus, without sacrificing accuracy much, energy balance can be calculated along stagnation line.

The energy balance is required for calculating the ratio of water that hits the surface and freezes, which is defined as freezing factor, n_0 . For rime ice the freezing factor is unity. For glaze ice, freezing factor is less than 1, and it is a parameter to be matched for ice accretion similitude.

$$n_{0,S} = n_{0,R} \quad (82)$$

$$n_0 = \left(\frac{c_{p,ws}}{\Lambda_f} \right) \left(\phi + \frac{\theta}{b} \right) \quad (83)$$

where $c_{p,ws} = 1.0074 \frac{\text{cal}}{\text{g K}}$ and $\Lambda_f = 79.7 \frac{\text{cal}}{\text{g}}$.

$$b = \frac{LWC V \beta_0 c_{p,ws}}{h_c} \quad (84)$$

$$h_c = \frac{k_a Nu_a}{L} \quad (85)$$

$$k_a = -12.69 \frac{\text{cal}}{\text{hr m K}} + 2.029 \frac{\text{cal}}{\text{hr m K}^{1.5}} \sqrt{T_{film}} \quad (86)$$

$$T_{film} = \frac{T_{st} + T_s}{2} \quad (87)$$

$$Nu_a = 1.14 Pr_a^{0.4} Re_a^{0.5} \quad (88)$$

$$Pr_a = \frac{c_{p,a} \mu_a}{k_a} \quad (89)$$

where $T_f = 273.15 \text{ K}$, $\Lambda_v = 597.3 \frac{\text{cal}}{\text{g}}$ and $c_{p,a} = 0.240 \frac{\text{cal}}{\text{g K}}$.

$$\phi = T_f - T_{st} - \frac{V^2}{2c_{p,ws}} \quad (90)$$

$$\theta = T_s - T_{st} - \frac{V^2}{2c_{p,a}} + \frac{h_G}{h_c} \Lambda_v \left(\frac{\frac{P_{ww}}{T_{st}} - \frac{P_{tot} P_w}{T_{tot} P_{st}}}{\frac{1}{0.622} \frac{P_{tot}}{T_{tot}} - \frac{P_{ww}}{T_{st}}} \right) \quad (91)$$

In the equation (91) the saturation pressure of vapor over water (P_w) and vapor pressure at the surface (P_{ww}), can be calculated using equation (92) that is taken from a curve fit that is provided in reference [32] that is valid for -50°C to 0°C .

Since P_{ww} is the vapor pressure at the surface, the surface temperature is used in equation (93) while calculating the temperature difference. For atmospheric vapor pressure, P_w , atmospheric static temperature is used in equation (93).

$$P_w = a_0 + \Delta T \left(a_1 + \Delta T \left(a_2 + \Delta T \left(a_3 + \Delta T \left(a_4 + \Delta T \left(a_5 + \Delta T a_6 \right) \right) \right) \right) \right) \quad (92)$$

$$\Delta T = T_{st,s} - 273.15 \text{ K} \quad (93)$$

$$P_{tot} = P_{st} \left(1 + \frac{\gamma - 1}{2} M^2 \right)^{\frac{\gamma}{\gamma - 1}} \quad (94)$$

$$h_G = \frac{h_c}{C_{p,a}} \left(\frac{Pr_a}{Sc_a} \right)^{0.67} \quad (95)$$

$$Sc_a = \frac{\mu_a}{\rho_a D_v} \quad (96)$$

$$D_v = 0.211 \frac{\text{cm}^2}{\text{s}} \left(\frac{T_{film}}{273.15 \text{ K}} \right)^{1.94} \left(\frac{101325 \text{ Pa}}{P_{st}} \right) \quad (97)$$

4.6. Surface-water dynamics similarity

For glaze ice a water film is present. The surface water dynamics affects the accreted ice shape. Weber number for reference and scaled conditions should be matched for surface-water dynamic similarity. The Weber number for characteristic length of the geometry is used for the current study. The characteristic length corresponds to the leading-edge radius which is proportional to the chord.

$$We_L = \frac{V^2 L \rho_a}{\sigma_{w/a}} \quad (98)$$

where $\sigma_{w/a} = 65 \text{ dyne/cm}$.

CHAPTER 5

ANALYSES

The numerical analyses are performed utilizing two different computational tools that are the 2-D in-house icing code AEROMSICE-2D and the commercial icing code FENSAP-ICE.

AEROMSICE-2D is in-house in-flight icing code that consists of panel method flow solver, Lagrangian droplet trajectory solver and ice accretion solver employing Extended Messinger Model [25].

FENSAP-ICE is an in-flight icing code that includes Euler droplet trajectory solver and ice accretion solver employing classical Messinger model [25]. Flow solution is provided by ANSYS® Fluent v18.0 CFD tool.

5.1. Analysis Set-up

In this part the options and input parameters that are supplied to the analysis tools are illustrated.

5.1.1. AEROMSICE-2D

The in-house code AEROMSICE-2D is a FORTRAN code that receives the inputs in a file .in in ascii format. In the input file the parameters to be specified by the use are listed in Table 5.1.

Table 5.1. *Input parameters for AEROMSICE-2D*

Parameters	
Angle of Attack (°)	
Number of elements	
Main airfoil chord length (m)	
Freestream velocity (m/s)	
Airfoil	NACA 4 or 5 digit series, airfoil coordinates input from airfoil.in
Number of coordinates for main airfoil and flap	
Airfoil names for main airfoil and flap	
Trajectory start and end locations (m)	
Trajectory step size (m)	0.0001
Flag for substrate temperature	Ts=Ta, Ts specified
substrate temperature (°C)	
Exposure time (s)	
Number of layers	(Number of steps that exposure time is divided)
Ice smoothing	not smoothed, smoothed
Smoothing level	1 (default)
Runback water	no runback, with runback
Roughness	computed with NASA 1, computed with NASA 2, user specified
Standard sand grain roughness (m)	0.001
Drag coefficient formulation	default law, extended default law
Breakup model	no breakup, breakup
Splash model	no splash, splash
Number of boundary-layer grids on each surface on each element	
Ambient parameters	
Temperature (°C)	
Pressure (Pa)	
LWC (g/m ³)	
MDV (µm)	
% Humidity	100 (default)

5.1.2. FENSAP-ICE

For ice accretion analysis, flow field solution, droplet trajectories, accumulation efficiencies and ice accretion are calculated for each flow condition. The cases that have long icing time are analyzed using multi-shot method that is dividing the icing time into smaller time steps. The solution is updated according to the ice shape formed after each step and the flow is resolved again with the current displaced geometry. This cycle is repeated until the total icing time is reached and the final ice shape is obtained.

5.1.2.1. Flow solution

CFD analysis is performed using ANSYS® Fluent v18.0 software. Assumptions and settings during analysis are given below:

- The simplifications required for the designed geometric models are made by using ANSYS Design Modeler v18.0 software and the mesh is created in the ANSYS v18.0 Meshing interface. A denser mesh is applied in the regions where ice accretion is expected.
- Pressure-based Navier-Stokes equations are solved in the Fluent Solver with ideal gas assumption.
- The viscosity of the air is formulated with the temperature dependent Sutherland approach.
- On finite volumes, transport equations are discretized using the second order upwind method.
- $k-\omega$ SST is used as the turbulence model.

For all analyses, the pressure and the specified temperature are provided as input to the velocity inlet or pressure-far-field type boundary condition. In addition, velocity or Mach number value and air flow direction are given as input to the same boundary condition. The surface is defined as the isothermal wall boundary condition. The use of the isothermal wall boundary condition is required by FENSAP-ICE to calculate heat transfer from the surface. In order to make this calculation, it is stated that the

surface temperature value should be several degrees above the stagnation temperature of the air and it is recommended in reference [3] to specify the surface temperature value as 10 degrees higher than the total temperature.

Surface roughness values are calculated in the Fluent Solver by NASA correlation. In order for FENSAP-ICE to use surface roughness output provided by Fluent, during the Fluent flow solution, the high roughness (icing) option should be used as the surface roughness model under the wall boundary condition [3]. The NASA correlation method used as a calculation method; characteristic length, flow speed and ambient temperature, LWC and surface roughness constant (taken as 0.5 according to Reference [3]) are inputs of roughness calculation.

5.1.2.2. Droplet trajectories

Droplet trajectories and ice accretion are calculated with ANSYS FENSAP-ICE software. The program options and input parameters for the calculations of droplet trajectories are stated in the following parts.

5.1.2.2.1. Model

The physical model and main particle parameters for droplet trajectories are stated in this part (Figure 5.1).

- The droplet particle type is chosen as droplets only and no crystals since the icing conditions that are analyzed are APPENDIX-C conditions, the supercooled droplet (SLD) option is also disabled likewise.
- The droplet drag model is chosen as default, water model that is mentioned at 2.1.

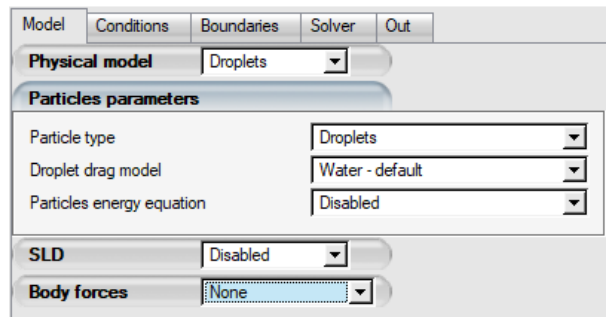


Figure 5.1. FENSAP-ICE software DROP3D Model Tab

5.1.2.2.2. Conditions

The ambient and droplet specific inputs are provided in conditions part. The reference conditions of corresponding icing conditions are stated in the conditions part (Figure 5.2).

- The droplet distribution choices are monodispersed, Langmuir B, C, D, E, from APPENDIX O and custom distribution. In this study the monodispersed droplet distribution is selected.

Model	Conditions	Boundaries	Solver	Out
Reference conditions				
Characteristic length		0.265	m	
Air velocity		82.17	m/s	
Air static pressure ▼		9.57003000e+004	Pa	
Air static temperature		265.9	K	
Reynolds number		1.6238e+006		
Mach number		2.5137e-001		
Adiabatic stagnation temperature		269.260278114	K	
Droplets reference conditions				
Choose Appendix	Disabled ▼	Configure...		
Liquid Water Content		1.32	g/m ³	
Droplet diameter		11.46	microns	
Water density		1000	kg/m ³	
Droplet distribution	Monodisperse ▼			
Get distribution				
Droplets initial solution Velocity components ▼				
Velocity X		81.9698	m/s	
Velocity Y		5.73189	m/s	
Velocity Z		0	m/s	
<input type="checkbox"/> Dry initialization				

Figure 5.2. FENSAP-ICE software DROP3D Conditions Tab

5.1.2.2.3. Boundaries

The boundaries part consists of the boundary conditions imported from the flow solver and the selection of droplet boundary conditions parameters to be imposed to the boundaries (Figure 5.3). The LWC and flow velocity components are input parameters for inlet boundary condition.

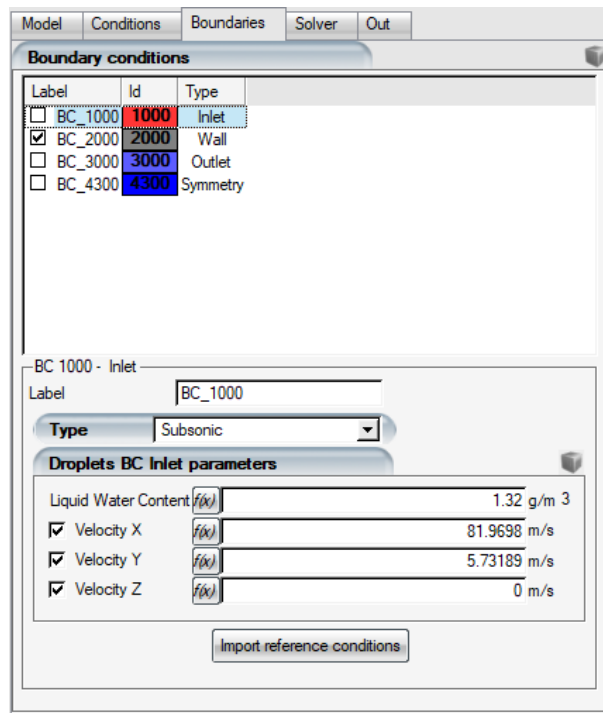


Figure 5.3. FENSAP-ICE software DRO3D Boundaries Tab

5.1.2.2.4. Solver

The solver part is where the iteration information is dictated to the program (Figure 5.4). The droplet trajectory calculations maximum number of time steps and CFL number are selected. A convergence criterion based on residuals may be designated.

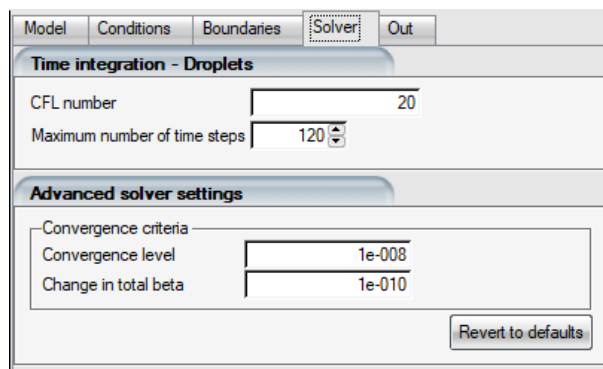


Figure 5.4. FENSAP-ICE software DRO3D Solver Tab

5.1.2.2.5. Out

The out part is where the decisions related to the outputs of droplet trajectory calculation are written is stated (Figure 5.5).

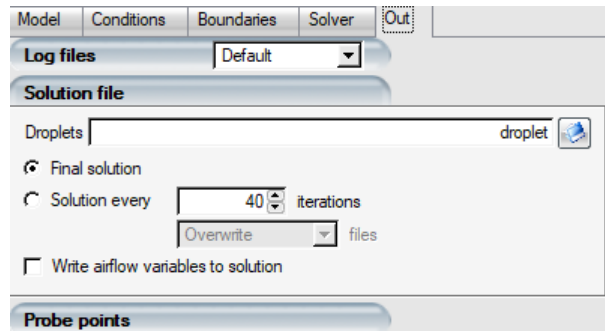


Figure 5.5. FENSAP-ICE software DROP3D Out Tab

5.1.2.3. Ice formation

The program options and input parameters for the calculations of ice formation are stated in the following parts.

5.1.2.3.1. Model

The physical model for ice accretion calculations are stated in this part (Figure 5.6). The Icing model permits the selection of ice-water model as rime ice glaze ice and water film. In this study, the glaze ice model is selected.

- Surface roughness is an important parameter for ice formation. Surface roughness values are calculated in the Fluent Solver by NASA correlation. Then beading model is employed in FENSAP-ICE solver [3].

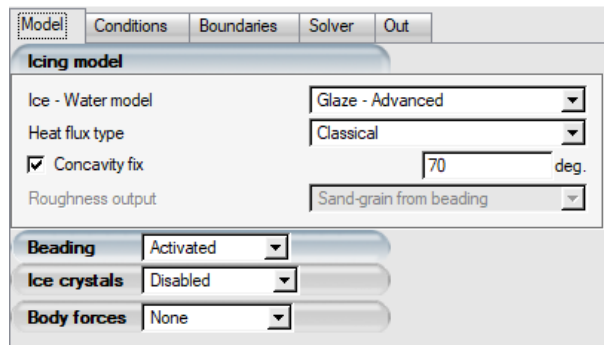


Figure 5.6. FENSAP-ICE software ICE3D Model Tab

5.1.2.3.2. Conditions

The conditions part for ice module includes the ambient, icing inputs that some of them are previously provided in conditions part in droplet module (Figure 5.7).

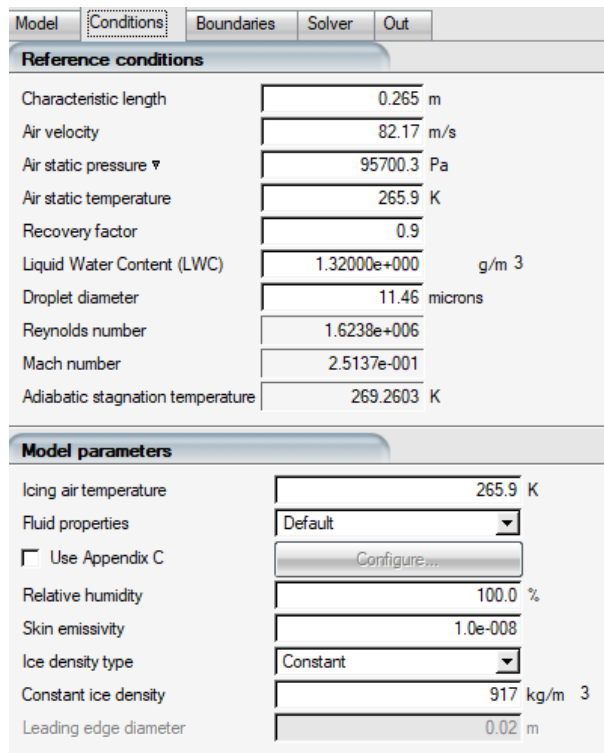


Figure 5.7. FENSAP-ICE software ICE3D Conditions Tab

The recovery factor is used to include the effect of the energy losses due to friction when computing the total temperature from the isentropic relations of the static temperature and the Mach number. Default value of recovery factor is unity that means the surface temperature is the stagnation temperature computed from freestream conditions. A recovery number less than one mean that the heat fluxes from flow solution are converted into convective heat transfer coefficients using the recovery reference temperature. The convective heat transfer coefficient is multiplied by the recovery ice temperature in the energy balance equation. An empirical formula to compute recovery factor for flat plate is $r = Pr^{1/3}$. When $Pr = 0.72$, laminar Prandtl number, the value for recovery factor is $r = 0.9$ which is the recommended value for icing prediction [2].

$$T_{tot,recovery} = T_{st} \left(1 + r \frac{\gamma - 1}{2} M^2 \right) \quad (99)$$

5.1.2.3.3. Boundaries

The boundary conditions imported from the flow solver and the selection of icing boundary conditions parameters to be imposed to the boundaries in this part (Figure 5.8). Whether icing is enabled for a certain wall or not is stated here. Moreover, heat flux may be imposed to the surface in this part for anti-icing or de-icing purposes which is out of the scope of this study.

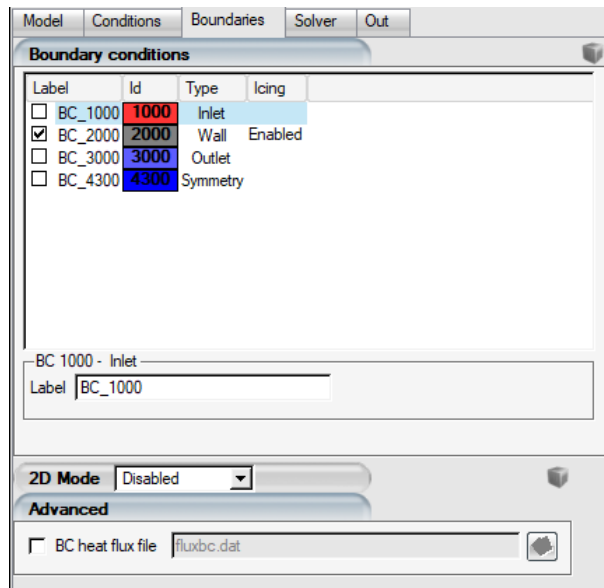


Figure 5.8. FENSAP-ICE software ICE3D Boundaries Tab

5.1.2.3.4. Solver

The total time of ice accretion and stop condition is selected in solver part (Figure 5.9). The stop condition may be total icing time as well as ice thickness. In this study, the total icing time is implied as stop condition.

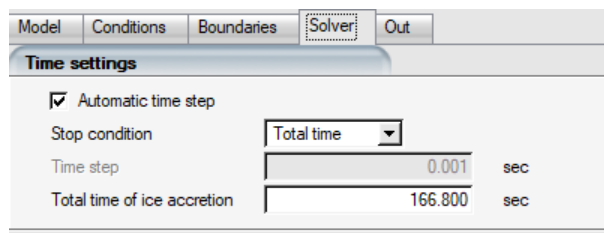


Figure 5.9. FENSAP-ICE software ICE3D Solver Tab

5.1.2.3.5. Out

The decisions about outputs of icing calculations are stated in out part (Figure 5.10). Additionally, the grid displacement options are provided in this part.

For mesh displacement due to ice accretion, FENSAP-ICE uses ALE (Arbitrary Lagrangian Eulerian) formulation. There are two displacement methods, coupled and uncoupled. The coupled method solves for the displacements in all directions simultaneously which yields good mesh orthogonally and element quality near the surface. Surface displacement due to ice accretion is obtained as an output from ICE3D.

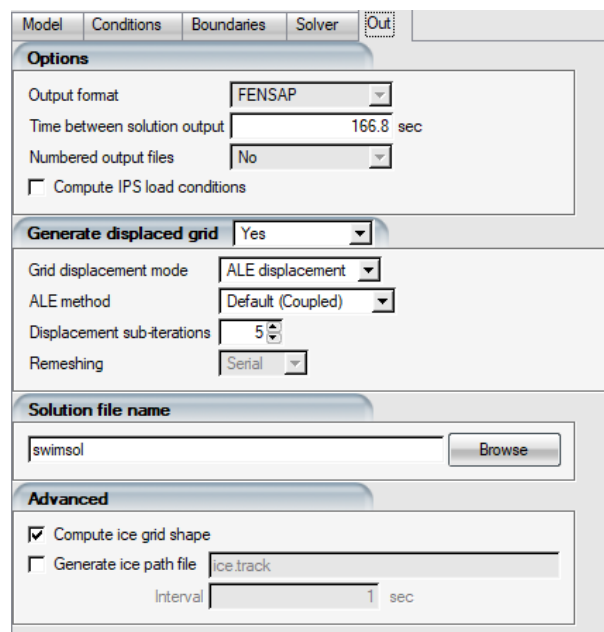


Figure 5.10. FENSAP-ICE software ICE3D Out Tab

5.2. Similitude Method

For current study scaling applications, Modified Ruff Method [1] which is a scaling method that is derived from similitude analysis with the addition of surface water dynamics similitude by matching Weber number, We_L is employed. Assuming that the geometry and flow similarity are achieved, the droplet trajectory similarity, the similarity of the total mass of liquid water hitting the surface, the energy balance similarity and surface-water dynamics similarity shall be ensured for the ice accretion

similitude. To provide that, modified inertia parameter (K_0), accumulation efficiency that is a function of modified inertia parameter (β_0), accumulation parameter (A_c), freezing rate (n_0), and droplet energy transfer parameter (ϕ) and Weber number (We_L) are to be matched. The scaling method inputs and outputs are given as a flowchart in Figure 5.11.

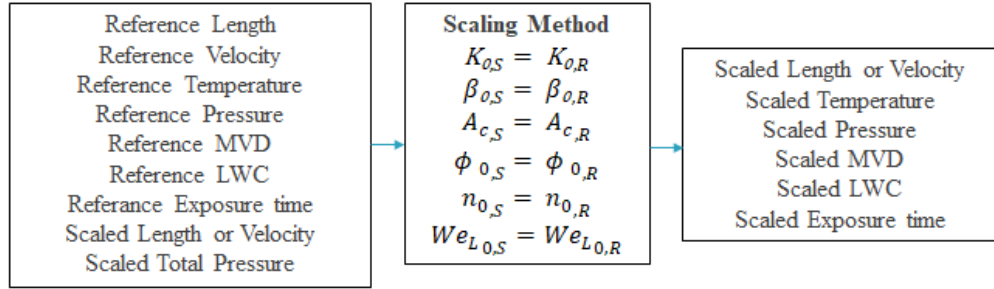


Figure 5.11. Flow chart for similitude method

The application of Modified Ruff Method with constant We_L is performed using MATLAB software. The atmospheric and scaling parameters are calculated for reference conditions. For size scaling, the desired scaled chord length is decided and with the scaled chord length input by equating the We_L values for reference and scaled cases, the scaled velocity may be obtained from equation (100 that is derived from equation (98).

$$V_S = V_S \sqrt{c_R/c_S} \quad (100)$$

After obtaining the scaled velocity, by equating the reference and scaled ϕ values, the T_{st} may be calculated as follows from equation (90):

$$T_{st,S} = T_f - \phi_S - V_S^2/2c_{p,ws} \quad (101)$$

Obtaining T_{st} , scaled Mach number and static pressure; total temperature may be calculated.

The following iteration is performed until a desired agreement between reference and scaled K_0 parameters is achieved. With the data obtained so far, the scaled droplet size may be determined iteratively to match the K_0 values. First guess for scaled droplet size, $\delta_{S,0}$, may be calculated as follows:

$$\frac{\delta_{S,0}}{\delta_R} = \left(\frac{d_S}{d_R}\right)^{0.617} \left(\frac{p_S}{p_R}\right)^{0.235} \left(\frac{V_S}{V_R}\right)^{-0.383} \left(\frac{T_S}{T_R}\right)^{0.235} \quad (102)$$

With the initial droplet diameter $\delta_{S,0}$, $K_{0S,0}$ is calculated. With these data, the droplet diameter of 1st iteration is as follows:

$$\delta_{S,1} = \delta_{S,0}(K_{0R}/K_{0S,0}) \quad (103)$$

$K_{0S,1}$ value is calculated using $\delta_{S,1}$ value. For 2nd iteration, the droplet diameter of is as follows:

$$\delta_{S,2} = \delta_{S,0} + (\delta_{S,1} - \delta_{S,0}) \left(\frac{K_{0R} - K_{0S,0}}{K_{0S,1} - K_{0S,0}} \right) \quad (104)$$

$K_{0S,2}$ value is calculated using $\delta_{S,2}$ value and the matching with reference value K_{0R} is checked for matching to two decimal places. If that is the case, the droplet diameter is decided. Then, the LWC value is determined by equating the freezing fraction n_0 values. This calculation is also an iteration process, the initial guess for LWC, $LWC_{S,0}$, is taken as the reference LWC value.

$$LWC_{S,0} = LWC_R \quad (105)$$

With the initial value $LWC_{S,0}$, $n_{0S,0}$ is calculated. The LWC value of 1st iteration is as follows:

$$LWC_{S,1} = LWC_{S,0} \left(\frac{n_{0S,0}}{n_{0R}} \right) \quad (106)$$

$n_{0S,1}$ value is calculated using $LWC_{S,1}$ value. For 2nd iteration, the LWC value is as follows:

$$LWC_{S,2} = LWC_{S,0} + (LWC_{S,1} - LWC_{S,0}) \left(\frac{n_{0S,0} - n_{0R}}{n_{0S,0} - n_{0S,1}} \right) \quad (107)$$

$n_{0S,2}$ value is calculated using $LWC_{S,2}$ value and the matching with reference value n_{0R} is checked. The agreement is assumed to be achieved when the difference between reference and scaled freezing fractions is less than 10% [1].

Since the scaled LWC value is obtained, by equating A_c values for reference and scaled cases, scaled exposure time is calculated from equation (81).

CHAPTER 6

RESULTS AND DISCUSSION

The purpose of the scaling method is to be able to obtain the conditions that results in the same ice shape as the reference ice shape and that can be provided in an icing wind tunnel when the full-scale reference values are not feasible to obtain or maintain. Thus, the analyses performed are also selected to serve this purpose. The main focus is on the size scaling and the velocity scaling considering the constrains of the test sections and limited range of test velocity.

Size and velocity scaling are performed for icing cases provided in [37] for airfoils NACA0012 and SA13112. The ice shapes and collection efficiencies for cases with airfoil NACA0012 are obtained by AEROMSICE-2D, in-house icing code, and FENSAP-ICE software. For a selected part of the cases, size-scaling of $\frac{1}{2}$ is performed on the reference conditions. When the geometry is scaled by $\frac{1}{2}$, the velocity for scaled geometry is increasing to match the surface-water dynamics by matching the Weber number. The MVD and the exposure time decreases to compensate the shrinkage of the geometry and to match the total water catch. The rest of the parameters are balanced by the relations of scaling equations.

For airfoil SA13112, ice shapes and collection efficiencies are obtained by FENSAP-ICE software. For these cases, velocity scaling to obtain lower test velocities is performed on reference conditions. For simplicity of obtaining geometry and mesh for the solution, the velocities are scaled such that it corresponds to model size scaling by 2 to match the Weber number. When the test velocity is decreased, the size of the scaled model increases and vice versa, since the velocity for scaled model is inversely proportional to size of the scaled model to match the surface-water dynamics which is provided by matching the Weber number. When the geometry is scaled by 2, the MVD

and the exposure time increases to compensate the enlargement of the geometry and to match the total water catch. The rest of the parameters are balanced by the relations of scaling equations.

For analysis with total icing time that is considered too long, the total icing time is divided into steps. The multistep icing calculations are performed by obtaining ice shape for initial step calculating flow field, droplet trajectories and ice accretion and repeating the procedure adopting resulting iced geometry as the new input geometry to successive step. The step sizes are decided according to computational data in [37], feasibility of re-meshing process and computational time and provided in the tables given in this chapter that introduce icing conditions.

Ice accretions obtained for cases 27, 28, 29, 30, 31, 32 whose conditions are given in Table 6.1 to Table 6.12 and ice shapes, C_p distributions and collection efficiencies given in Figure 6.1 to Figure 6.6 are for NACA0012 airfoil at 4° angle of attack, velocities are in incompressible range and ambient temperature increases from case 27 to case 32. Thus, from case 27 to case 32 the icing characteristics are expected to go from rime to glaze.

Ice accretions obtained for cases 33, 34, 35, 36 whose conditions are given in Table 6.13 to Table 6.20 and ice shapes, C_p distributions and collection efficiencies given in Figure 6.7 to Figure 6.10 are for NACA0012 airfoil at 4° angle of attack, velocities are just above incompressible range and ambient temperature increases from case 33 to case 36. Thus, from case 27 to case 32 the icing characteristics are expected to go from rime to glaze.

Thus, for cases 27 to 32, the icing characteristics with increasing ambient temperature is investigated for low velocities where incompressible flow assumption is valid.

For cases 33 to 36, the icing characteristics with increasing ambient temperature shall be investigated. For these cases the velocities are higher compared to the previous cases, that compressibility effects are starting to be observed in the flow.

Ice accretions obtained for case 39 whose conditions are given in Table 6.21 and Table 6.22 and ice shapes, C_p distributions and collection efficiencies given in Figure 6.11 are for NACA0012 airfoil at 8° angle of attack, velocity is higher than previous cases, thus in compressible range and the angle of attack is twice as the previous cases. For this specific case the icing characteristics in compressible range at higher angle of attack shall be investigated.

Ice accretions obtained for case 40 whose conditions are given in Table 6.23 and Table 6.24 and ice shapes, C_p distributions and collection efficiencies given in Figure 6.12, are for SA13112 airfoil at 10° angle of attack, velocity is in incompressible range the effect of high angle of attack shall be investigated.

Ice accretions obtained for cases, 41, 42, * whose conditions are given in Table 6.25 to Table 6.30 and ice shapes, C_p distributions and collection efficiencies given in Figure 6.13 to Figure 6.15 are for SA13112 airfoil at 0° angle of attack at high velocities. For these cases the icing characteristics at high velocities shall be investigated.

For cases 27 to 39, size of the geometry is scaled $\frac{1}{2}$ and for cases 40, 41, 42 and *, velocity are scaled such that the scaled geometry is 2 times of the reference geometry. This method is chosen for simplicity of geometry creation and meshing.

The results that are obtained by in-house code AEROMSICE-2D are designated by “Reference” and “Scaled” while the results obtained by FENSAP-ICE are designated as “reference FENSAP” and “scaled FENSAP”. Experimental data, if present, are included to all comparison as “Exp”. In addition, for some cases, computational results from the literature are added.

The initial C_p distribution shows good agreement between reference and scaled cases that can be interpreted as good agreement in initial flow field prediction. The initial collection efficiency distributions show also good agreement between reference and scaled cases that can be interpreted as good agreement in droplet trajectory calculations.

Table 6.1. Case 27 icing conditions for reference and scaled cases in reference [37]

Case	Type	c, m	M	Re _a , 10 ⁴	T _{st} , °C	P _s , (kPa)	V, m/s	MVD, μm	LWC, g/m ³	t _{exp} , s	# of Steps
27	Ref.	0.53	0.185	8.39	-27.80	95.610	58.10	20.00	1.30	480.00	4
	Scaled	0.265	0.262	5.93	-28.20	95.341	82.17	11.44	1.48	149.54	2

Table 6.2. Case 27 scaling parameters for reference and scaled cases in reference [37]

Case	Type	K ₀	β ₀	A _c	b	φ, K	θ, K	n ₀	We _L , 10 ⁶
27	Ref.	1.81	0.68	2.36	0.55	27.55	34.07	1.13	0.87
	Scaled	1.81	0.68	2.36	0.53	27.55	32.70	1.13	0.87

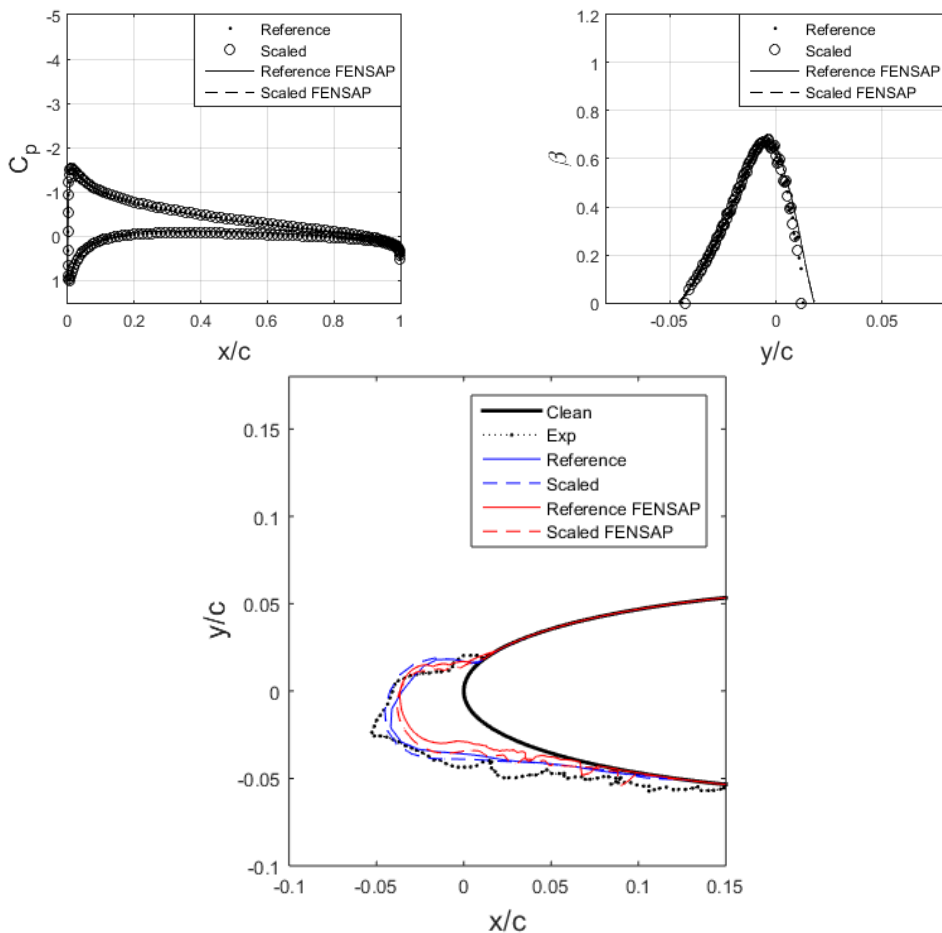


Figure 6.1. Case 27 C_p distributions, collection efficiencies and ice shapes obtained by analyses and experiments in reference [37] for NACA0012 airfoil at 4° AOA

Ice accretions obtained for Case 27 whose conditions are given in Table 6.1 and Table 6.2 and ice shapes given in Figure 6.1 show rime ice characteristics that is also in agreement with the stagnation freezing fraction, n_0 , being above unity which corresponds to unity physically. The velocity is in incompressible range and the ice is rime, thus, this case is expected to have better ice accretion predictions.

The scaling parameters selected to be matched are matched in the desired confidence level. The scaling method accurately predicts ice shape for scaled case compared with the reference case. Both computational tools satisfy the similitude of scaled and reference ice shape.

Table 6.3. Case 28 icing conditions for reference and scaled cases in reference [37]

Case	Type	c, m	M	Re _a , 10 ⁴	T _{st} , °C	P _{st} , (kPa)	V, m/s	MVD, μm	LWC, g/m ³	t _{exp} , s	# of Steps
28	Ref.	0.53	0.182	7.92	-19.80	95.610	58.10	20.00	1.30	480.00	4
	Scaled	0.265	0.258	5.61	-20.20	95.484	82.17	11.45	1.46	151.39	2

Table 6.4. Case 28 scaling parameters for reference and scaled cases in reference [37]

Case	Type	K ₀	β ₀	A _c	b	φ, K	θ, K	n ₀	We _L , 10 ⁶
28	Ref.	1.80	0.68	2.36	0.56	19.55	25.21	0.82	0.87
	Scaled	1.80	0.68	2.36	0.53	19.55	23.86	0.82	0.87

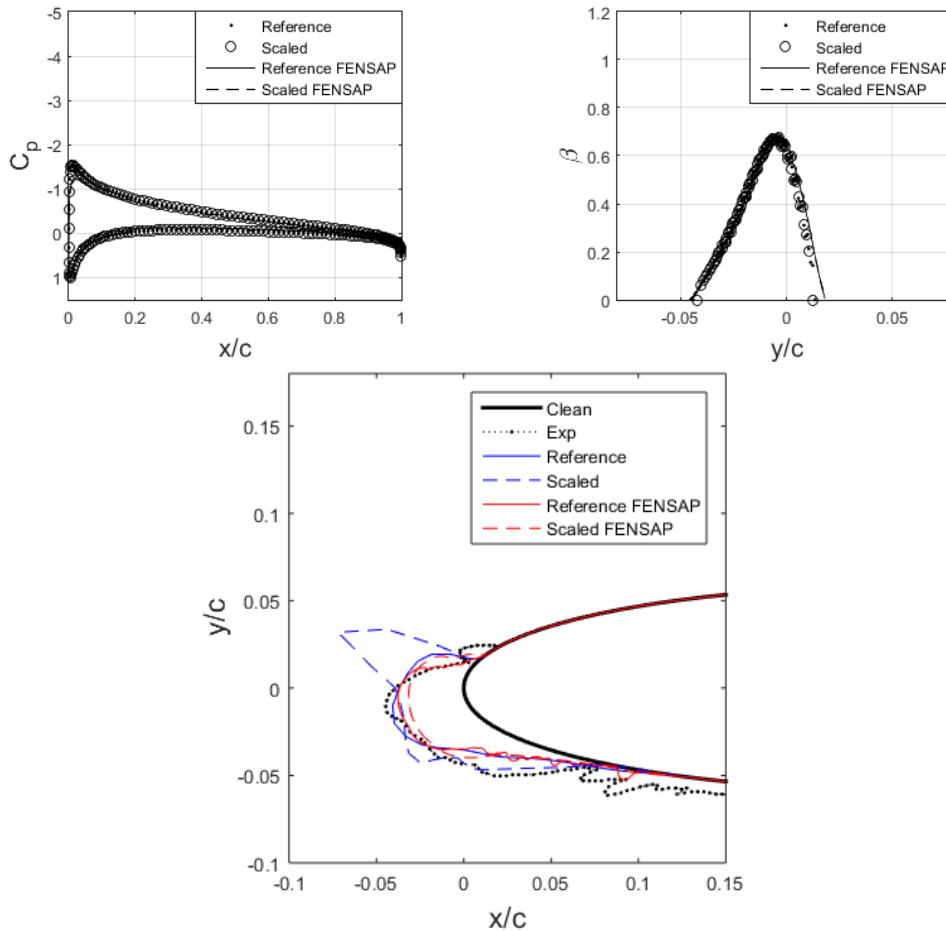


Figure 6.2. Case 28 Cp distributions, collection efficiencies and ice shapes obtained by analyses and experiments in reference [37] for NACA0012 airfoil at 4° AOA

Ice accretions obtained for Case 28 whose conditions are given in

Table 6.3 and Table 6.4 and ice shapes given in Figure 6.2 show mixed ice characteristics that is also in agreement with the stagnation freezing fraction, n_0 , being below unity which corresponds to mixed or glaze ice. The ice accretion shows both rime and glaze ice characteristics, thus, it is mixed ice case.

The scaling parameters selected to be matched are matched in the desired confidence level. The scaling method accurately predicts ice shape for scaled case comparing with the reference case. FENSAP-ICE satisfies the similitude of scaled and reference ice shape adequately. There is a horn in AEROMSICE-2D scaled ice shape that is not present for experimental data and results of other analysis. This may be due to the loss of accuracy of the computational tool for small MVD values which is the case for scaled icing condition.

Table 6.5. Case 29 icing conditions for reference and scaled cases in reference [37]

Case	Type	c, m	M	Re _a , 10 ⁴	T _{st} , °C	P _{st} , (kPa)	V, m/s	MVD, μm	LWC, g/m ³	t _{exp} , s	# of Steps
29	Ref.	0.53	0.180	7.60	-13.90	95.610	58.10	20.00	1.30	480.00	4
	Scaled	0.265	0.255	5.39	-14.30	95.584	82.17	11.46	1.43	154.26	2

Table 6.6. Case 29 scaling parameters for reference and scaled cases in reference [37]

Case	Type	K ₀	β ₀	A _c	b	φ, K	θ, K	n ₀	We _L , 10 ⁶
29	Ref.	1.79	0.68	2.36	0.56	13.65	18.18	0.58	0.87
	Scaled	1.79	0.68	2.36	0.52	13.65	16.85	0.58	0.87

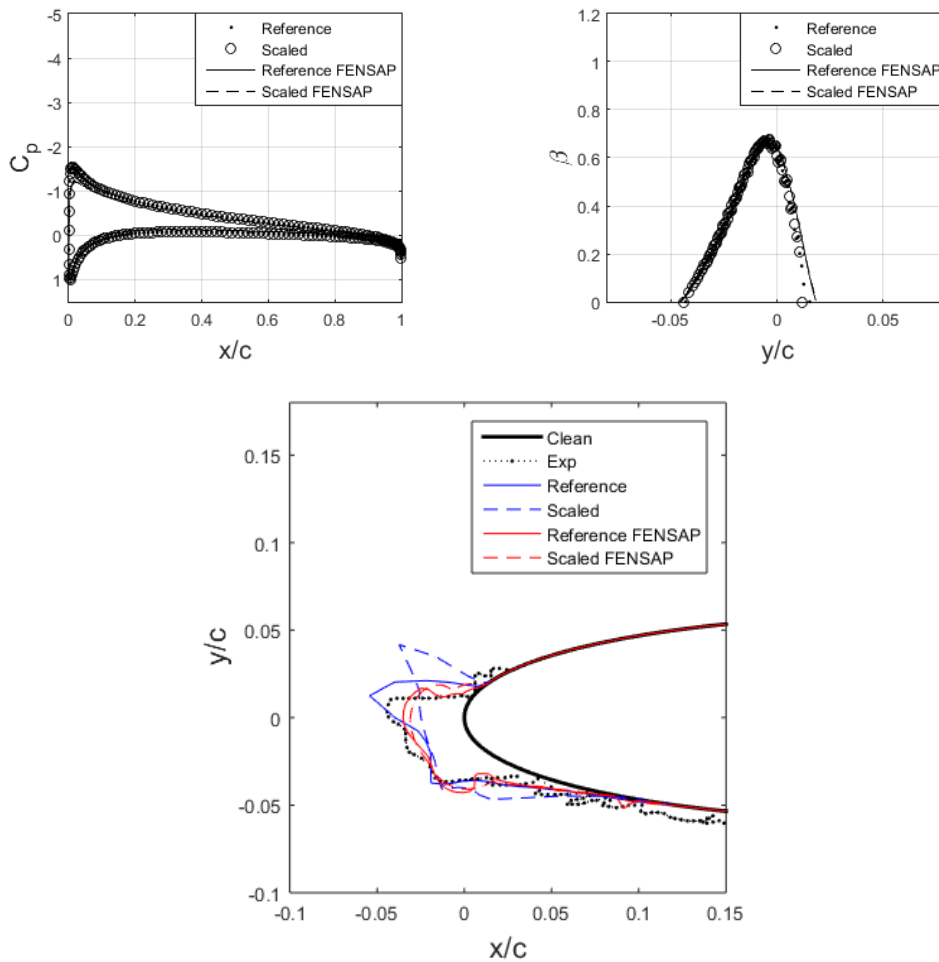


Figure 6.3. Case 29 Cp distributions, collection efficiencies and ice shapes obtained by analyses and experiments in reference [37] for NACA0012 airfoil at 4° AOA

For ice accretions given in Figure 6.3 for Case 29 whose conditions are given in Table 6.5 and Table 6.6 show glaze ice characteristics that is also in agreement with the stagnation freezing fraction, n_0 , being below unity which corresponds to glaze ice.

The scaling parameters selected to be matched are matched in the desired confidence level. The scaling method accurately predicts ice shape for scaled case comparing with the reference case. FENSAP-ICE satisfies the similitude of scaled and reference ice shape with a slight over-smoothing of the horn that can be observed in the experiment.

AEROMSICE-2D reference and scaled ice shapes have different horn angles. This may be due to the limitation of the computational tool for small MVD values since the reference case with MVD of 20 μm results in good agreement with the experimental data.

Table 6.7. Case 30 icing conditions for reference and scaled cases in reference [37]

Case	Type	c, m	M	Re _a , 10 ⁴	T _{st} , °C	P _{st} , (kPa)	V, m/s	MVD, μm	LWC, g/m ³	t _{exp} , s	# of Steps
30	Ref.	0.53	0.178	7.24	-6.70	95.610	58.10	20.00	1.30	480.00	4
	Scaled	0.265	0.251	5.14	-7.10	95.700	82.17	11.46	1.32	166.81	2

Table 6.8. Case 30 scaling parameters for reference and scaled cases in reference [37]

Case	Type	K ₀	β ₀	A _c	b	φ, K	θ, K	n ₀	We _L , 10 ⁶
30	Ref.	1.79	0.68	2.36	0.57	6.45	8.66	0.27	0.87
	Scaled	1.79	0.68	2.36	0.49	6.45	7.40	0.27	0.87

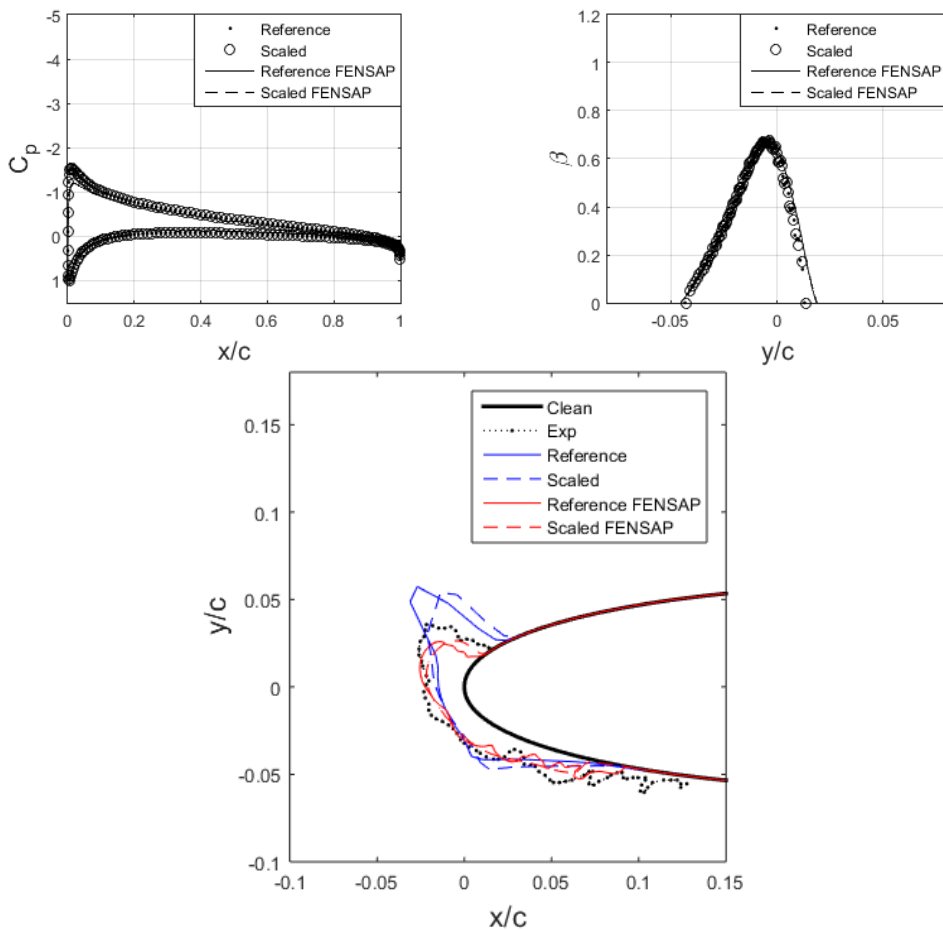


Figure 6.4. Case 30 C_p distributions, collection efficiencies and ice shapes obtained by analyses and experiments in reference [37] for NACA0012 airfoil at 4° AOA

Table 6.9. Case 31 icing conditions for reference and scaled cases in reference [37]

Case	Type	c, m	M	Re _a , 10 ⁴	T _{st} , °C	P _{st} , (kPa)	V, m/s	MVD, μm	LWC, g/m ³	t _{exp} , s	# of Steps
31	Ref.	0.53	0.177	7.10	-3.90	95.610	58.10	20.00	1.30	480.00	4
	Scaled	0.265	0.250	5.04	-4.30	95.744	82.17	11.47	1.13	195.64	2

Table 6.10. Case 31 scaling parameters for reference and scaled cases in reference [37]

Case	Type	K ₀	β ₀	A _c	b	φ, K	θ, K	n ₀	We _L , 10 ⁶
31	Ref.	1.78	0.68	2.36	0.57	3.65	4.58	0.15	0.87
	Scaled	1.78	0.68	2.36	0.42	3.65	3.36	0.15	0.87

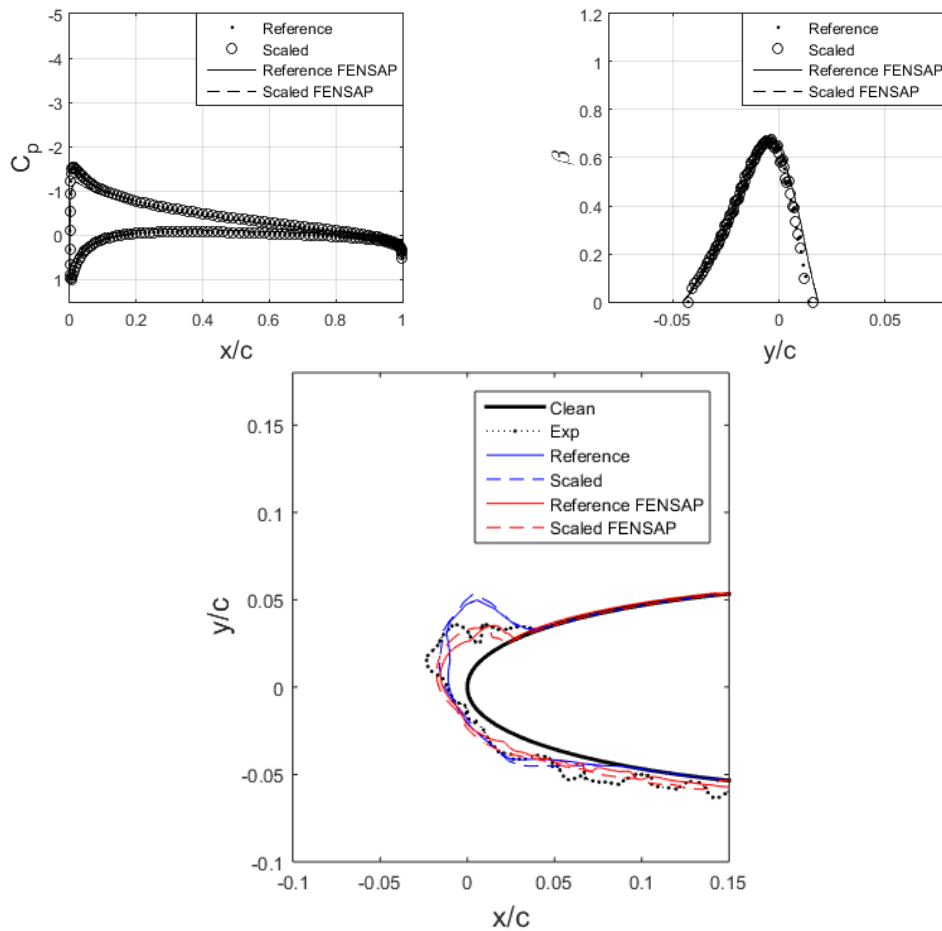


Figure 6.5. Case 31 C_p distributions, collection efficiencies and ice shapes obtained by analyses and experiments in reference [37] for NACA0012 airfoil at 4° AOA

For ice accretions given in Figure 6.4, Figure 6.5 for cases 30 and 31 whose conditions are given in Table 6.7 to Table 6.10 show glaze ice characteristics that is also in agreement with the stagnation freezing fraction, n_0 , being below unity which corresponds to glaze ice.

The scaling parameters selected to be matched are matched in the desired confidence level. The scaling method accurately predicts ice shape for scaled case comparing with the reference case. FENSAP-ICE and AEROMSICE-2D satisfy the similitude of scaled and reference ice shape, adequately with small deviations. AEROMSICE-2D slightly overpredicts the horn geometry while FENSAP-ICE underpredicts it compared to experiment.

Table 6.11. Case 32 icing conditions for reference and scaled cases in reference [37]

Case	Type	c, m	M	Re _a , 10 ⁴	T _{st} , °C	P _{st} , (kPa)	V, m/s	MVD, μm	LWC, g/m ³	t _{exp} , s	# of Steps
32	Ref.	0.53	0.176	7.05	-2.80	95.610	58.10	20.00	1.30	480.00	4
	Scaled	0.265	0.250	5.01	-3.20	95.761	82.17	11.47	0.85	259.89	3

Table 6.12. Case 32 scaling parameters for reference and scaled cases in reference [37]

Case	Type	K ₀	β ₀	A _c	b	φ, K	θ, K	n ₀	We _L , 10 ⁶
32	Ref.	1.78	0.68	2.36	0.57	2.55	2.91	0.10	0.87
	Scaled	1.78	0.68	2.36	0.31	2.55	1.70	0.10	0.87

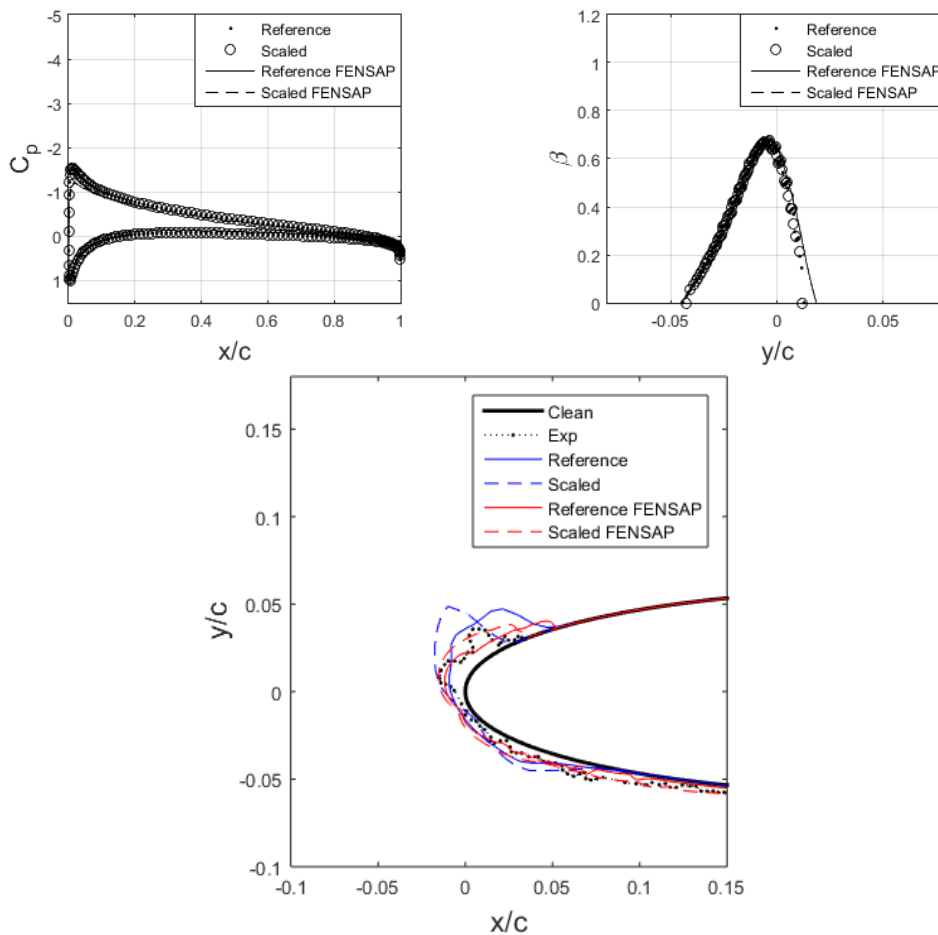


Figure 6.6. Case 32 C_p distributions, collection efficiencies and ice shapes obtained by analyses and experiments in reference [37] for NACA0012 airfoil at 4° AOA

For ice accretions given in Figure 6.6 for case 32 whose conditions are given in Table 6.11 to Table 6.12 show glaze ice characteristics that is also in agreement with the stagnation freezing fraction, n_0 , being below unity which corresponds to glaze ice.

The scaling parameters selected to be matched are matched in the desired confidence level. The scaling method predicts ice shape for scaled case comparing with the reference case quite accurately. However, FENSAP-ICE predicts slightly more ice on upper side for scaled case compared to the reference case.

For AEROMSICE-2D, the scaled ice shape has a horn shape that is not present for the reference case. As mentioned before, this might be due to the loss of accuracy of the computational tool when MVD is smaller than 15 microns.

Table 6.13. Case 33 icing conditions for reference and scaled cases in reference [37]

Case	Type	c, m	M	Re _a , 10 ⁴	T _{st} , °C	P _{st} , (kPa)	V, m/s	MVD, μm	LWC, g/m ³	t _{exp} , s	# of Steps
33	Ref.	0.53	0.300	13.32	-30.50	92.060	93.89	20.00	1.05	372.00	4
	Scaled	0.265	0.426	9.10	-31.55	88.256	132.78	11.27	1.10	125.03	1

Table 6.14. Case 33 scaling parameters for reference and scaled cases in reference [37]

Case	Type	K ₀	β ₀	A _c	b	φ, K	θ, K	n ₀	We _L , 10 ⁶
33	Ref.	2.43	0.74	2.39	0.62	29.60	34.30	1.07	2.27
	Scaled	2.43	0.74	2.39	0.56	29.60	30.97	1.07	2.27

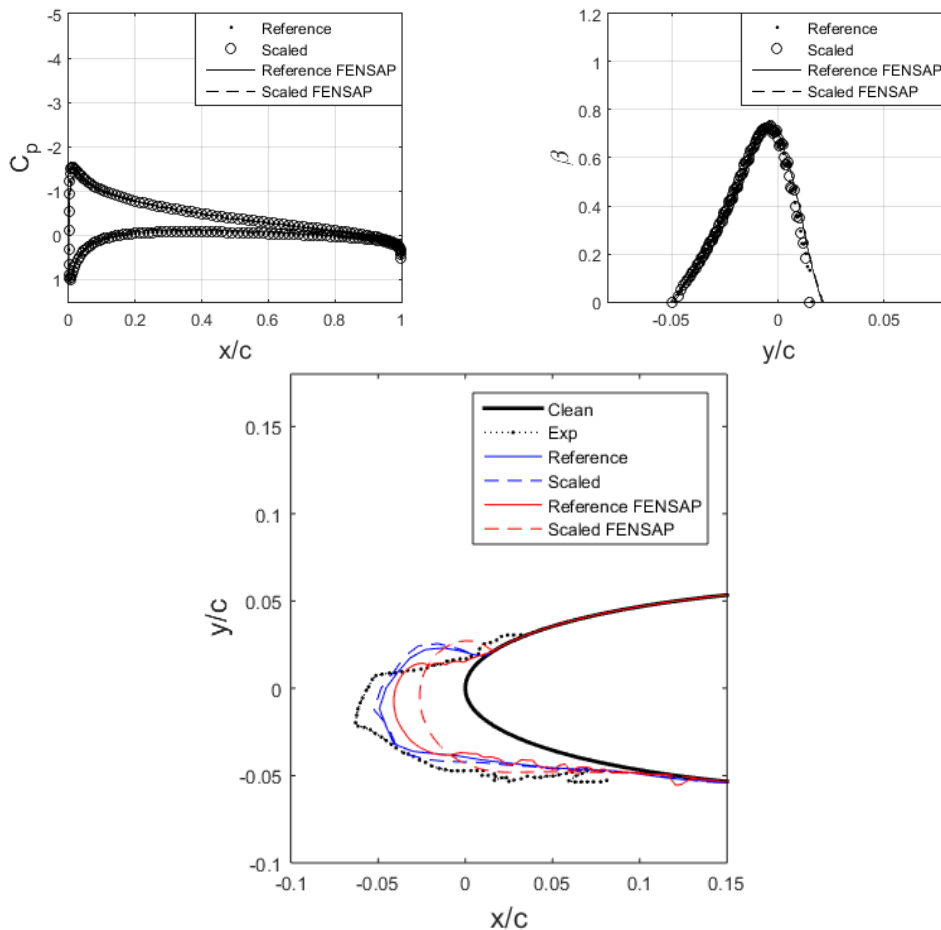


Figure 6.7. Case 33 Cp distributions, collection efficiencies and ice shapes ice shapes obtained by analyses and experiments in reference [37] for NACA0012 airfoil at 4° AOA

For ice accretions given in Figure 6.7 for Case 33 whose conditions are given in Table 6.13 and Table 6.14 show rime ice characteristics that is also in agreement with the stagnation freezing fraction, n_0 , being above unity which corresponds to unity physically. The velocity is in incompressible range and the ice is rime, thus, this case is expected to have better ice accretion predictions.

The scaling parameters selected to be matched are matched in the desired confidence level. Both AEROMSICE-2D and FENSAP-ICE underpredicts ice height compared to the experiment. While there is a good agreement between scaled and reference ice shapes for AEROMSICE-2D, scaled ice shape prediction of FENSAP-ICE is not well-matched with reference ice shape, that might be due to over-smoothing.

The scaling method accurately predicts ice shape for scaled case comparing with the reference case. AEROMSICE-2D satisfy the similitude of scaled and reference ice shape.

Table 6.15. Case 34 icing conditions for reference and scaled cases in reference [37]

Case	Type	c , m	M	Re_a , 10^4	T_{st} , $^{\circ}C$	P_{st} , (kPa)	V, m/s	MVD, μm	LWC, g/m^3	t_{exp} , s	# of Steps
34	Ref.	0.53	0.293	12.05	-16.60	92.060	93.89	20.00	1.05	372.00	2
	Scaled	0.265	0.415	8.29	-17.65	88.848	132.78	11.31	1.01	136.28	2

Table 6.16. Case 34 scaling parameters for reference and scaled cases in reference [37]

Case	Type	K_0	β_0	A_c	b	ϕ , K	θ , K	n_0	We_L , 10^6
34	Ref.	2.42	0.74	2.39	0.64	15.70	18.77	0.57	2.27
	Scaled	2.42	0.74	2.39	0.52	15.70	15.49	0.57	2.27

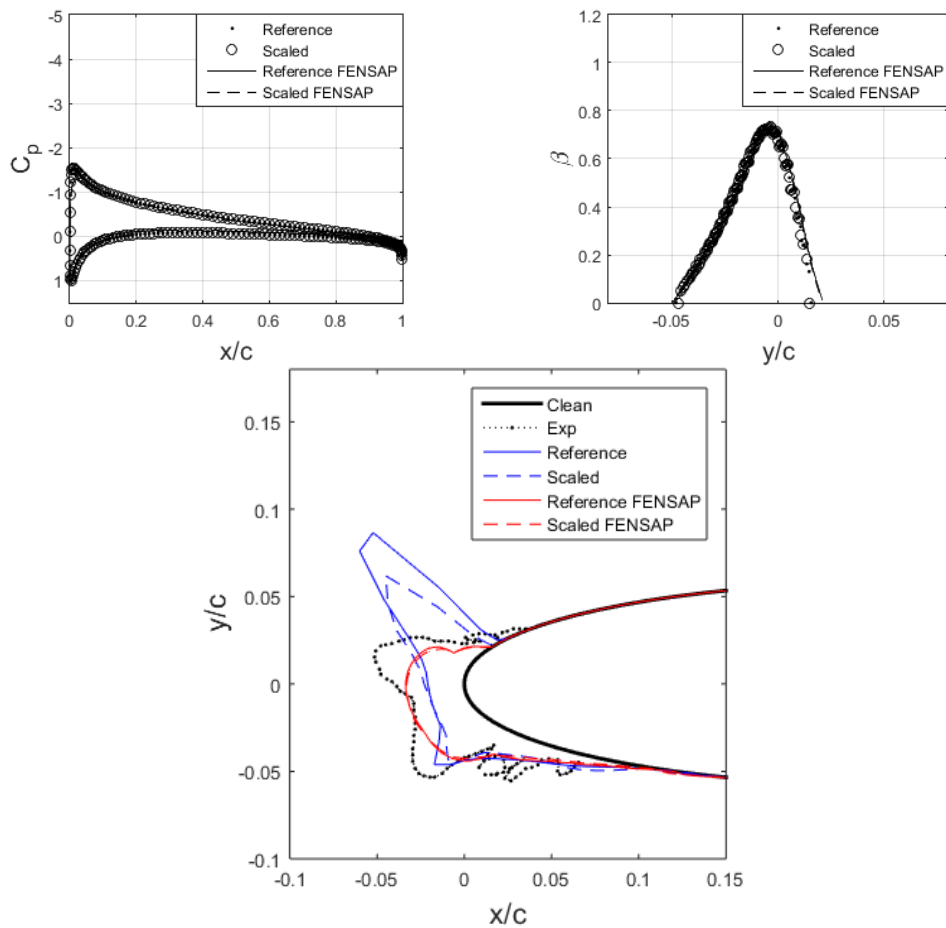


Figure 6.8. Case 34 C_p distributions, collection efficiencies and ice shapes obtained by analyses and experiments in reference [37] for NACA0012 airfoil at 4° AOA

For ice accretions given in Figure 6.8 for Case 34 whose conditions are given in Table 6.15 and Table 6.16 show glaze ice characteristics that is also in agreement with the stagnation freezing fraction, n_0 , being below unity which corresponds to glaze ice.

The scaling parameters selected to be matched are matched in the desired confidence level. The scaling method accurately predicts ice shape for scaled case comparing with the reference case. FENSAP-ICE satisfies the similitude of scaled and reference ice shape with an under-prediction of horn shapes that is due to the over-smoothing of the tool.

AEROMSICE-2D overpredicts the horn geometry, that may be due to the compressible effects are starting to affect the flow field and ice prediction, especially for glaze ice, becomes challenging.

Table 6.17. Case 35 icing conditions for reference and scaled cases in reference [37]

Case	Type	c , m	M	Re_a , 10^4	T_{st} , °C	P_{st} , (kPa)	V, m/s	MVD, μm	LWC, g/m^3	t_{exp} , s	# of Steps
35	Ref.	0.53	0.290	11.69	-12.20	92.060	93.89	20.00	1.05	372.00	3
	Scaled	0.265	0.411	8.05	-13.25	89.023	132.78	11.31	0.93	149.29	2

Table 6.18. Case 35 scaling parameters for reference and scaled cases in reference [37]

Case	Type	K_0	β_0	A_c	b	ϕ , K	θ , K	n_0	We_L , 10^6
35	Ref.	2.42	0.74	2.39	0.64	11.30	13.30	0.41	2.27
	Scaled	2.42	0.74	2.39	0.48	11.30	10.07	0.41	2.27

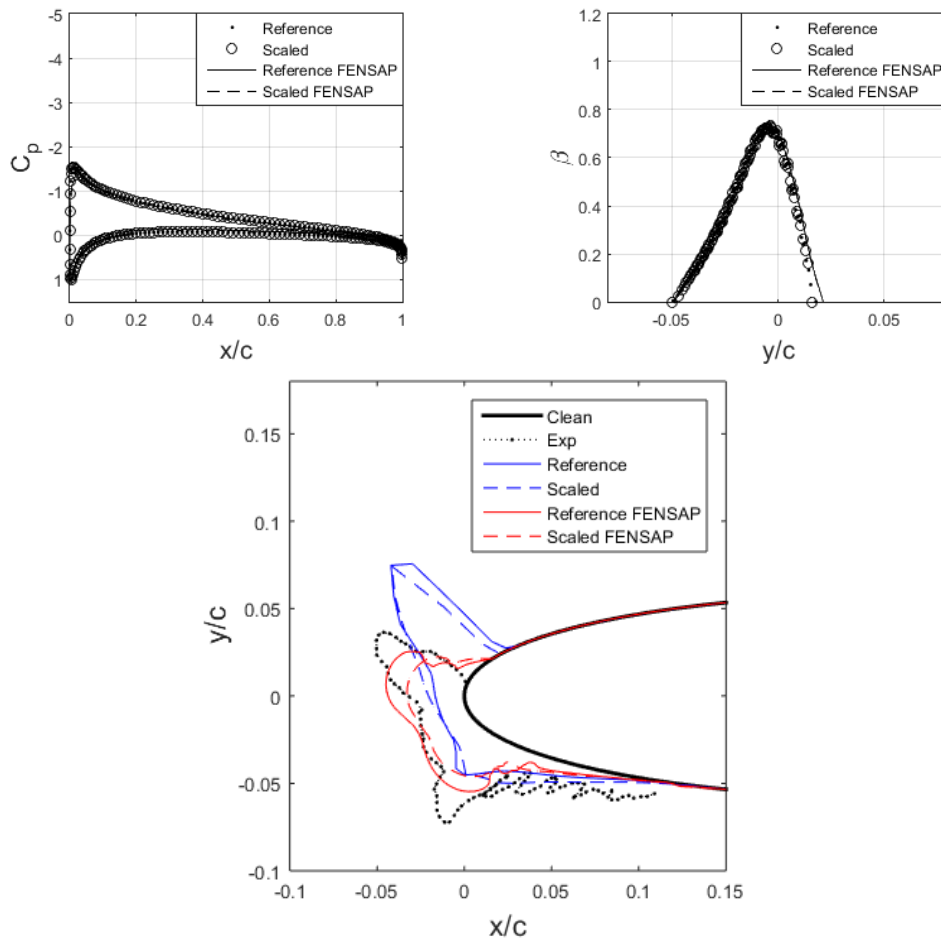


Figure 6.9. Case 35 C_p distributions, collection efficiencies and ice shapes obtained by analyses and experiments in reference [37] for NACA0012 airfoil at 4° AOA

For ice accretions given in Figure 6.9 for Case 35 whose conditions are given in Table 6.17 and Table 6.18 show glaze ice characteristics that is also in agreement with the stagnation freezing fraction, n_0 , being below unity which corresponds to glaze ice.

The scaling parameters selected to be matched are matched in the desired confidence level. The scaling method accurately predicts ice shape for scaled case comparing with the reference case. FENSAP-ICE and AEROMSICE-2D satisfy the similitude of scaled and reference ice shape quite adequately. However, for results of FENSAP-ICE, horns are under-predicted for scaled ice shape compared with the reference case. This may be due to the increase of velocity for scaled case, the compressibility may have an effect on the scaled ice shape, causing a deviation from reference ice shape.

For AEROMSICE-2D, even though the correlation between reference and scaled ice shapes is good, both predictions have deviation from experimental ice shape with a difference of horn angle. That may be due to the method that computational tool employs is not as reliable when the compressibility effects are present.

Table 6.19. Case 36 icing conditions for reference and scaled cases in reference [37]

Case	Type	c, m	M	Re _a , 10 ⁴	T _{st} , °C	P _{st} , (kPa)	V, m/s	MVD, μm	LWC, g/m ³	t _{exp} , s	# of Steps
36	Ref.	0.53	0.287	11.25	-6.60	92.060	93.89	20.00	1.05	372.00	4
	Scaled	0.265	0.407	7.77	-7.65	89.238	132.78	11.33	0.55	249.73	2

Table 6.20. Case 36 scaling parameters for reference and scaled cases in reference [37]

Case	Type	K ₀	β ₀	A _c	b	φ, K	θ, K	n ₀	We _L , 10 ⁶
36	Ref.	2.42	0.74	2.39	0.64	5.70	5.72	0.18	2.27
	Scaled	2.42	0.74	2.39	0.29	5.70	2.56	0.18	2.27

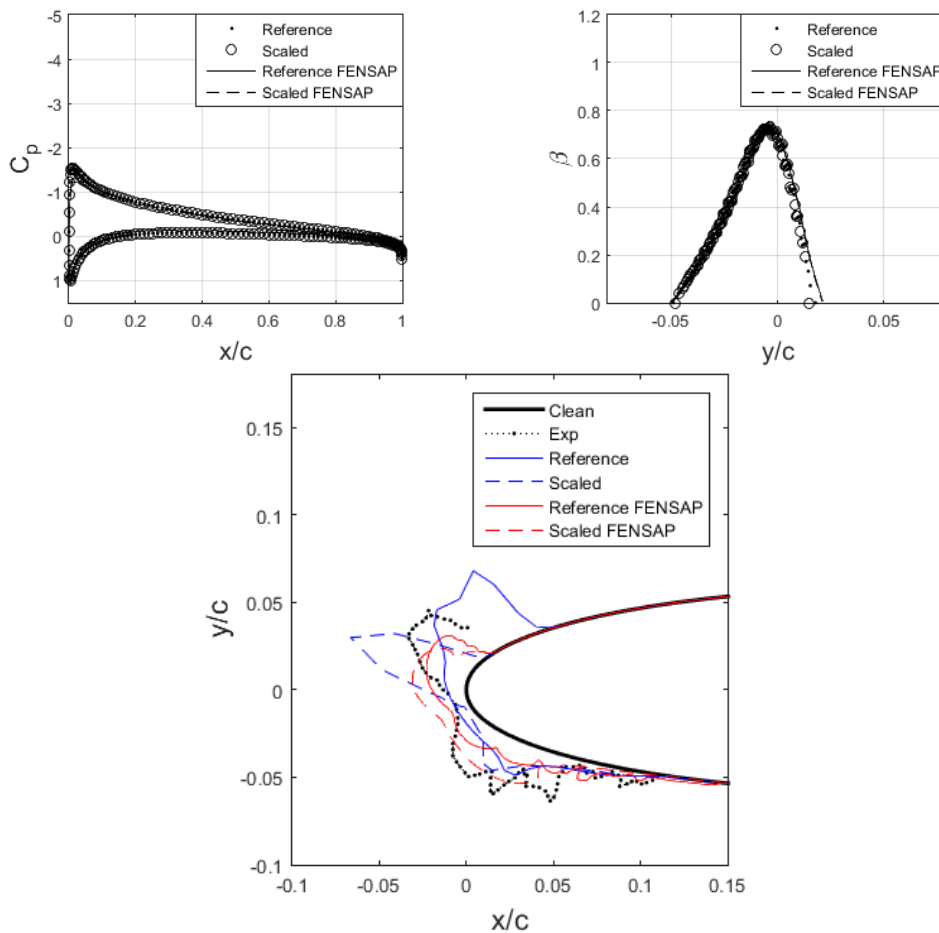


Figure 6.10. Case 36 C_p distributions, collection efficiencies and ice shapes obtained by analyses and experiments in reference [37] for NACA0012 airfoil at 4° AOA

For ice accretions given in for Figure 6.10 Case 36 whose conditions are given in

Table 6.19 and Table 6.20 show glaze ice characteristics that is also in agreement with the stagnation freezing fraction, n_0 , being below unity which corresponds to glaze ice.

The scaling parameters selected to be matched are matched in the desired confidence level. The scaling method accurately predicts ice shape for scaled case comparing with the reference case. FENSAP-ICE satisfies the similitude of scaled and reference ice shape with a slight difference of ice thickness for scaled case.

The results show reference ice shape upper limit is overpredicted and scaled ice shape horn height is overpredicted by AEROMSICE-2D, that may be explained by the compressible effects are starting to affect the flow field.

Table 6.21. Case 39 icing conditions for reference and scaled cases in reference [37]

Case	Type	c , m	M	Re_a , 10^4	T_{st} , $^{\circ}C$	P_{st} , (kPa)	V , m/s	MVD, μm	LWC, g/m^3	t_{exp} , s	# of Steps
39	Ref.	0.53	0.400	14.29	-3.90	85.000	131.50	20.00	0.60	180.00	2
	Scaled	0.265	0.568	9.69	-5.95	80.360	185.97	11.22	2.94	13.00	1

Table 6.22. Case 39 scaling parameters for reference and scaled cases in reference [37]

Case	Type	K_0	β_0	A_c	b	ϕ , K	θ , K	n_0	We_L , 10^6
39	Ref.	3.03	0.77	0.92	0.48	2.00	-2.68	-0.05	4.45
	Scaled	3.03	0.77	0.92	2.02	2.00	-8.73	-0.03	4.45

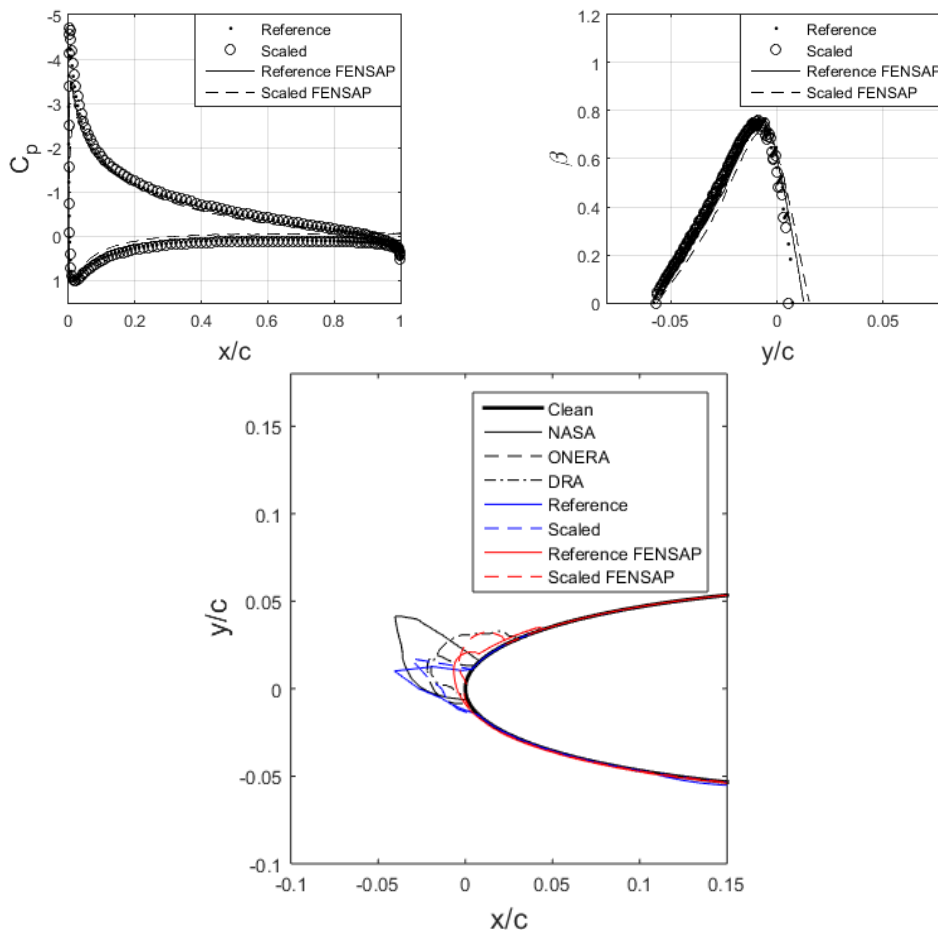


Figure 6.11. Case 39 C_p distributions, collection efficiencies and ice shapes obtained by analyses in reference [37] for NACA0012 airfoil at 8° AOA

For ice accretions given in Figure 6.11 for Case 39 whose conditions are given in Table 6.21 and Table 6.22 show glaze ice characteristics that is also in agreement with the stagnation freezing fraction, n_0 , being below zero which corresponds to glaze ice with high velocity that is the case when there is no icing in the stagnation but there is runback icing near stagnation.

The scaling parameters selected to be matched are matched in the desired confidence level. The scaling method accurately predicts ice shape for scaled case comparing with the reference case. FENSAP-ICE and AEROMSICE-2D satisfy the similitude of scaled and reference ice shape with some error. Since the case is in compressible regime and has glaze ice characteristics, the prediction of ice accretion is also challenging besides application of scaling.

There is no available experimental result. Thus, when the results of current study are compared with numerical results in the literature. The ice shape characteristics resemble, however; DRA and FENSAP-ICE obtain circular, smoother ice shapes, whereas, NASA, ONERA and AEROMSICE-2D obtain pointy, sharper ice shapes. The reference and scaled results are in good agreement among each other.

Table 6.23. Case 40 icing conditions for reference and scaled cases in reference [37]

Case	Type	c, m	M	Re _a , 10 ⁴	T _{st} , °C	P _{st} , (kPa)	V, m/s	MVD, μm	LWC, g/m ³	t _{exp} , s	# of Steps
40	Ref.	0.60	0.250	9.7	-10.00	79.500	81.30	20.00	0.50	900.00	3
	Scaled	1.20	0.177	16.9	-9.61	97.85	57.49	36.88	0.47	2682.87	4

Table 6.24. Case 40 scaling parameters for reference and scaled cases in reference [37]

Case	Type	K ₀	β ₀	A _c	b	φ, K	θ, K	n ₀	We _L , 10 ⁶
40	Ref.	2.08	0.71	2.10	0.31	9.37	12.36	0.62	1.93
	Scaled	2.08	0.71	2.10	0.32	9.37	12.59	0.62	1.93

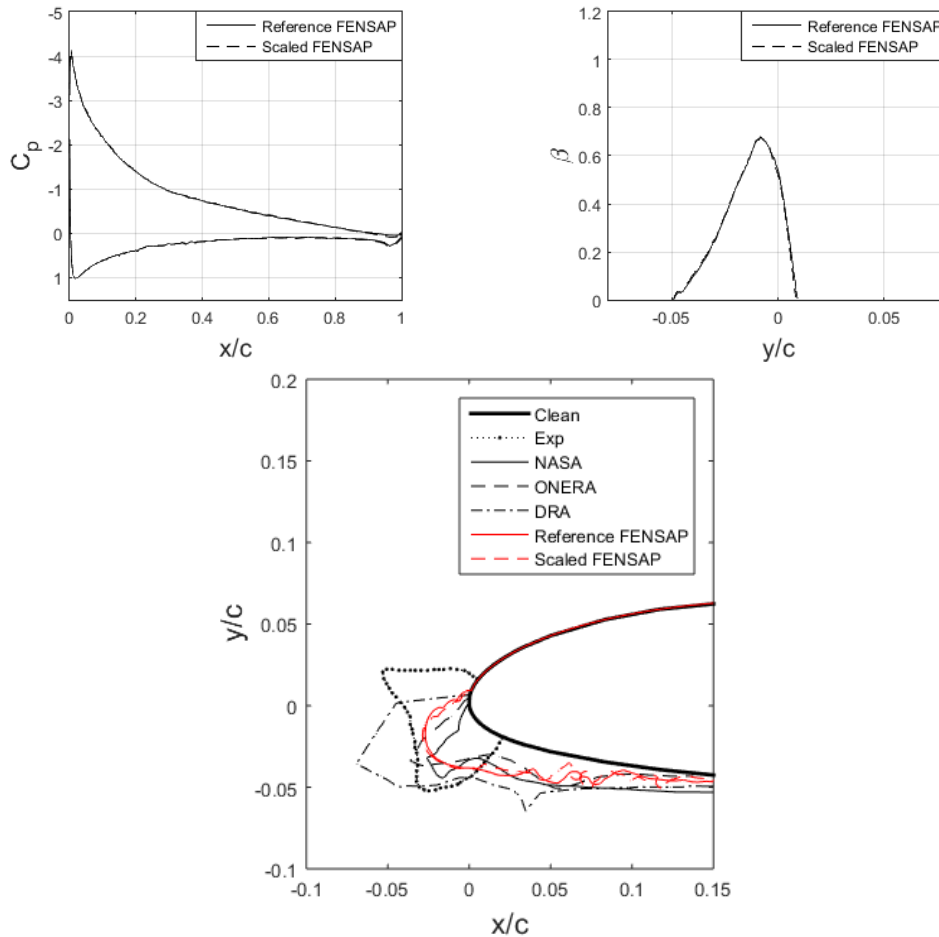


Figure 6.12. Case 40 Cp distributions, collection efficiencies and ice shapes obtained by analyses and experiments in reference [37] for SA13112 airfoil at 10° AOA

For the cases given for SA13112 airfoil, the main focus is on velocity scaling. The size for scaled geometry is increasing to match the surface-water dynamics, Weber number. The MVD and the exposure time increases to compensate the growth of the geometry and to match the total water catch. The rest of the parameters are balanced by the relations of scaling equations.

For ice accretions given in Figure 6.12 for Case 40 whose conditions are given in Table 6.23 and Table 6.24 show mixed ice characteristics that is also in agreement with the stagnation freezing fraction, n_0 , being below unity which corresponds to mixed or glaze ice.

The scaling parameters selected to be matched are matched in the desired confidence level. The scaling method accurately predicts ice shape for scaled case comparing with the reference case. FENSAP-ICE satisfies the similitude of scaled and reference ice shape adequately.

The final ice shapes obtained by NASA, ONERA and FENSAP-ICE are well-matched. DRA overpredicts the ice accretion compared to other numerical analyses results, however, still the ice shapes are similar. Reference and scaled ice shapes are also in good agreement among each other, however, neither limits of experimental ice nor its shape match the numerical results.

Table 6.25. Case 41 icing conditions for reference and scaled cases in reference [37]

Case	Type	c, m	M	Re _a , 10 ⁴	T _{st} , °C	P _{st} , (kPa)	V, m/s	MVD, μm	LWC, g/m ³	t _{exp} , s	# of Steps
41	Ref.	0.60	0.500	19.49	-10.00	79.500	162.50	20.00	0.50	450.00	4
	Scaled	1.20	0.352	31.48	-8.43	91.772	114.90	36.77	1.12	570.75	3

Table 6.26. Case 41 scaling parameters for reference and scaled cases in reference [37]

Case	Type	K ₀	β ₀	A _c	b	φ, K	θ, K	n ₀	We _L , 10 ⁶
41	Ref.	3.11	0.78	2.10	0.49	7.02	1.60	0.13	7.70
	Scaled	3.11	0.78	2.10	1.20	7.02	5.94	0.15	7.70

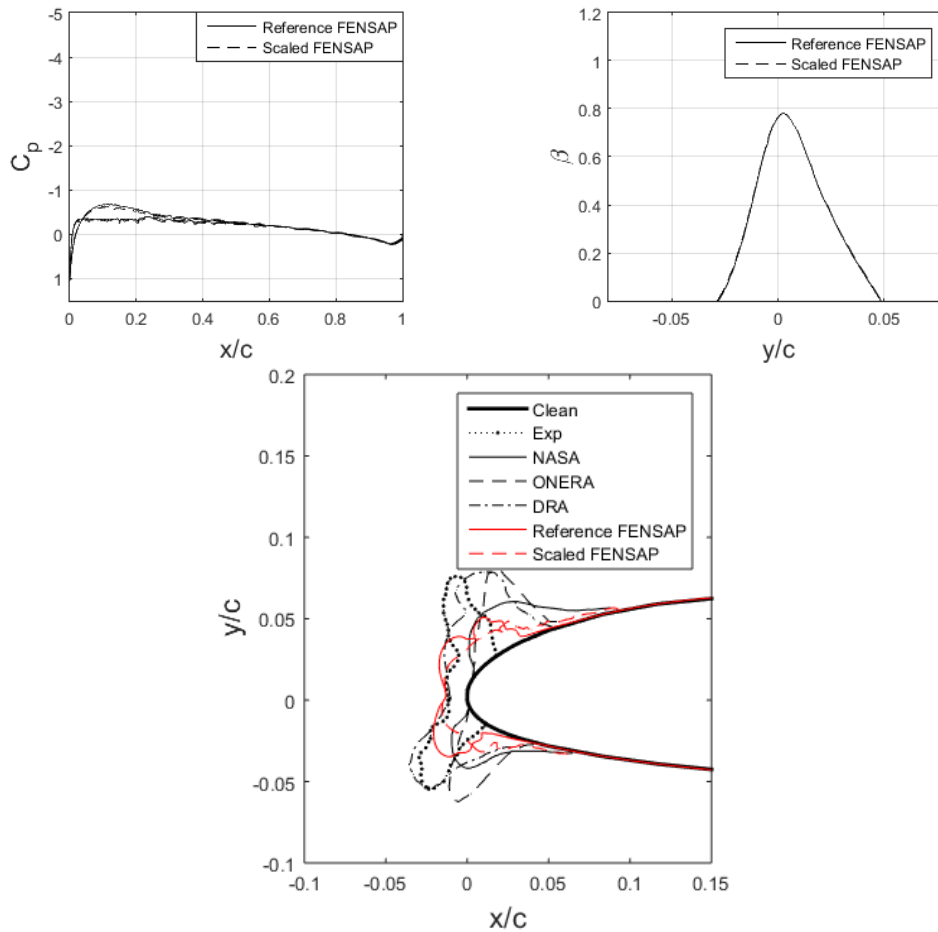


Figure 6.13. Case 41 C_p distributions, collection efficiencies and ice shapes obtained by analyses and experiments in reference [37] for SA13112 airfoil at 0° AOA

For ice accretions given in Figure 6.13 for Case 41 whose conditions are given in Table 6.25 and Table 6.26 show glaze ice characteristics that is also in agreement with the stagnation freezing fraction, n_0 , being below unity which corresponds to glaze ice.

The scaling parameters selected to be matched are matched in the desired confidence level. The scaling method accurately predicts ice shape for scaled case comparing with the reference case. FENSAP-ICE satisfies the similitude of scaled and reference ice shape with a small under-prediction of horns for scaled ice case.

The ice height and limits of ice obtained by FENSAP-ICE are similar to experimental ice. However, the horns are underpredicted for both scaled and reference cases. That may be explained by the over-smoothing on done by the computational tool.

Table 6.27. Case 42 icing conditions for reference and scaled cases in reference [37]

Case	Type	c , m	M	Re_a , 10^4	T_{st} , $^{\circ}C$	P_{st} , (kPa)	V, m/s	MVD, μm	LWC, g/m^3	t_{exp} , s	# of Steps
42	Ref.	0.600	0.80	34.53	-30.2	79.500	249.90	20.0	0.50	180	3
	Scaled	1.200	0.561	48.28	-26.4	80.750	176.71	35.7	0.96	266	3

Table 6.28. Case 42 scaling parameters for reference and scaled cases in reference [37]

Case	Type	K_0	β_0	A_c	b	ϕ , K	θ , K	n_0	We_L , 10^6
42	Ref.	3.919	0.811	1.294	0.610	22.747	6.053	0.413	18.22
	Scaled	3.919	0.811	1.294	1.387	22.747	18.703	0.458	18.22

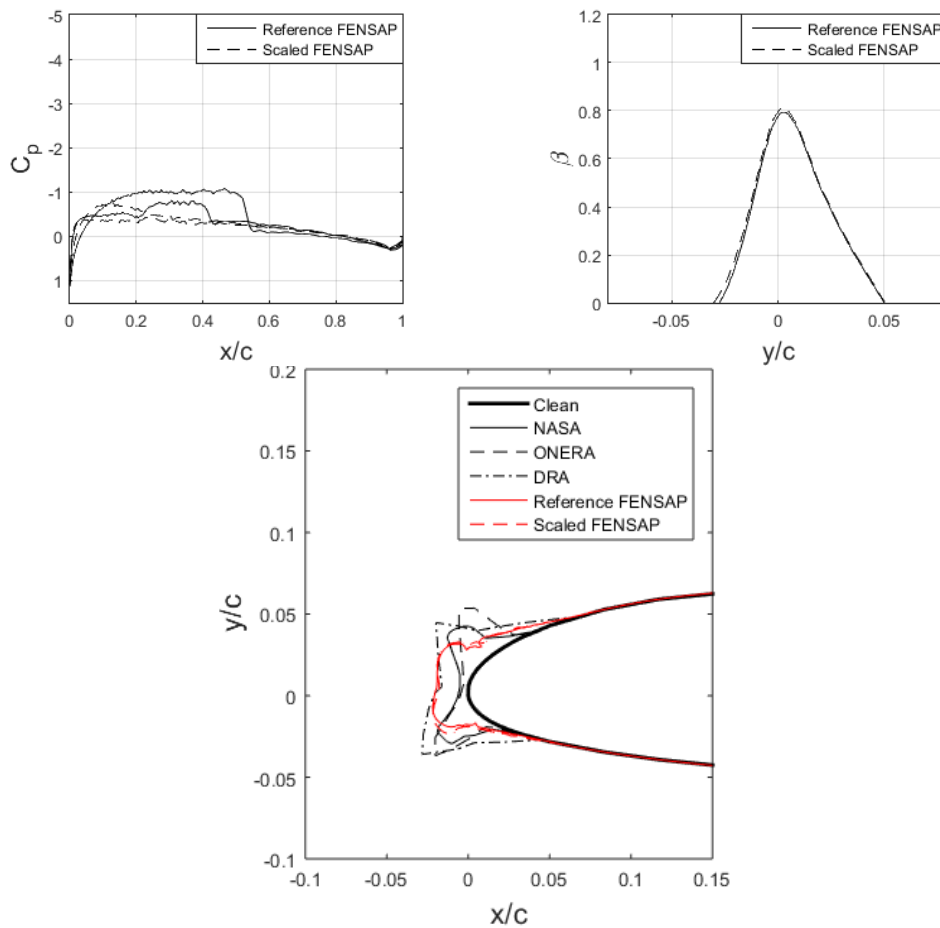


Figure 6.14. Case 42 C_p distributions, collection efficiencies and ice shapes obtained by analyses in reference [37] for SA13112 airfoil at 0° AOA

For ice accretions given in Figure 6.14 for Case 42 whose conditions are given in Table 6.27 and Table 6.28 show glaze ice characteristics that is also in agreement with the stagnation freezing fraction, n_0 , being below unity which corresponds to glaze ice.

The scaling parameters selected to be matched are matched in the desired confidence level. The scaling method accurately predicts ice shape for scaled case comparing with the reference case. FENSAP-ICE satisfies the similitude of scaled and reference ice shape.

There are no experimental results available but numerical results in the literature are presented. The ice limits of all ice shapes obtained by numerical analyses are similar. The ice height obtained by FENSAP-ICE is well matched with ice shape obtained by NASA.

Table 6.29. Case * icing conditions

Case	Type	c, m	M	Re _a , 10 ⁴	T _{st} , °C	P _{st} , (kPa)	V, m/s	MVD, μm	LWC, g/m ³	t _{exp} , s	# of Steps
*	Ref.	0.533	0.750	17.92	-10.0	54.890	243.90	20.0	0.12	900	3
	Scaled	0.800	0.610	30.63	-7.6	77.820	199.08	30.9	0.08	2519	4

Table 6.30. Case * scaling parameters

Case	Type	K ₀	β ₀	A _c	b	φ, K	θ, K	n ₀	We _L , 10 ⁶
*	Ref.	5.112	0.844	1.705	0.176	2.948	-14.915	-1.038	15.41
	Scaled	5.111	0.844	1.705	0.108	2.948	-9.042	-1.026	15.41

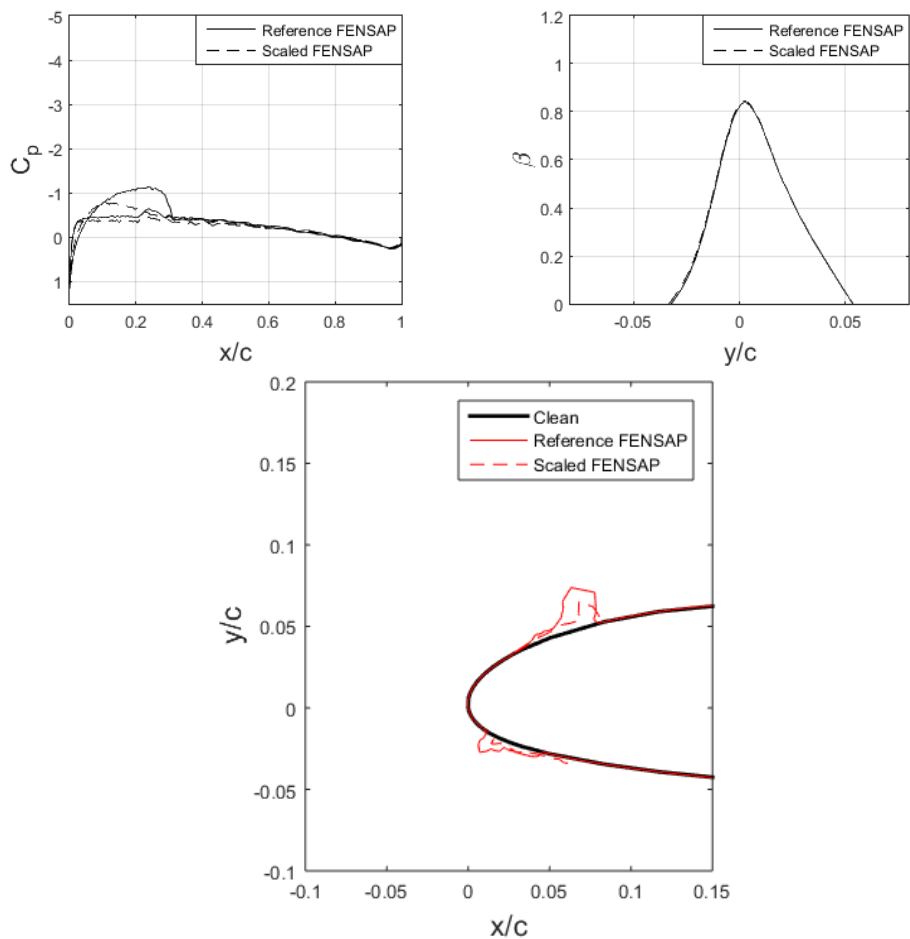


Figure 6.15. Case * ice shapes obtained by analyses for SA13112 airfoil at 0° AOA

For ice accretions given in Figure 6.15 for Case * whose conditions are given in Table 6.29 and Table 6.30 show glaze ice characteristics that is also in agreement with the stagnation freezing fraction, n_0 , being below zero which corresponds to glaze ice with high velocity that is the case when there is no icing in the stagnation but there is runback icing near stagnation. The case is in compressible regime and has glaze ice characteristics with runback ice, the prediction of ice accretion is also challenging besides application of scaling.

The scaling parameters selected to be matched are matched in the desired confidence level. The scaling method accurately predicts ice shape for scaled case comparing with the reference case. FENSAP-ICE satisfies the similitude of scaled and reference ice shape adequately even though that is a challenging case.

There are no experimental and numerical results available in the literature since the reference condition is not selected from the literature. The case is chosen as a challenging velocity scaling case. The scaled and reference ice shapes and limits obtained by FENSAP-ICE are in good agreement.

6.1. CONCLUSION

This study presents an icing scaling method that is utilized to scale the model size or selected reference icing condition to perform the icing test with scaled conditions that lies in the range of capabilities of existing icing wind tunnels and to obtain the same ice shape as the reference. The scaling method is introduced as Modified Ruff Method that satisfies the similitude by guaranteeing geometric, flow field, droplet trajectory, water catch, energy balance and surface water dynamics similarities. The method is implemented for both model size scaling and velocity scaling.

The method is applied to several cases having APPENDIX-C icing conditions present in the literature. The final ice shapes are obtained by in-house icing code AEROMSICE-2D and commercial icing software FENSAP-ICE.

Final ice geometries and collection efficiencies obtained by numerical analyses for both reference and scaled icing cases are compared among themselves and with experimental and numerical data present in the literature.

The collection efficiencies obtained for both numerical tools show good agreement even though the solution methods for flow field and droplet trajectory are different.

The ice shapes for scaled and reference conditions obtained by the same solver usually well-matched. The resulting ice shapes obtained by AEROMSICE-2D and FENSAP-ICE also have good agreement, however, AEROMSICE-2D usually overpredicts the horns and FENSAP-ICE underpredicts and smoothens the horns.

The numerical results obtained in current study by both numerical tools show good agreement with experimental and numerical data in literature with a few exceptions. For rime ice cases the agreement of ice shapes is satisfying. The cases that do not have good agreement are usually glaze ice cases that ice shapes are hard to predict. Since glaze ice have more complex icing physics, the prediction and scaling of ice shapes are both challenging. To conclude, the overall agreement is fair considering the ice accretion limits on geometries and maximum ice thickness.

The scaling method works well considering the agreement of the results for reference and scaled ice geometries. However, it should be kept in mind that there could be phenomena for 3D case that may disrupt the correlation.

The success of scaling method for cases that have 3D effects such as swept wings and cases including heating systems are to be investigated for future studies.

REFERENCES

- [1] Anderson, D. N., Manual of Scaling Method, Technical Report, March 2004.
- [2] ANSYS® FENSAP-ICE, Release 18.2, Help System, Theory Guide, ANSYS, Inc.
- [3] ANSYS FENSAP-ICE Tutorial Guide, 2017.
- [4] ANSYS® Fluent, Release 15.0, Help System, Theory Guide, ANSYS, Inc.
- [5] Armand, C., Techniques and Facilities Used at the Onera Modane Centre for Icing Tests, North Atlantic Treaty Organization Advisory Group for Aerospace Research and Development, AGARD-AF-127, November 1978.
- [6] Beaugendre, H., Morency, F., & Habashi, W. G., FENSAP-ICE's three-dimensional in-flight ice accretion module: ICE3D. *Journal of Aircraft*, 40(2), 239-247, 2003.
- [7] Bourgault, Y., Beaugendre, H. and Habashi, W.G., Development of a Shallow Water Icing Model in FENSAP-ICE, *Journal of Aircraft*, 37, pp. 640-646, 2000.
- [8] Bourgault, Y., Habashi, W., Dompierre, J., Boutanios, Z., Di Bartolomeo, W., An Eulerian approach to supercooled droplets impingement calculations. In 35th Aerospace Sciences Meeting and Exhibit (p. 176), 1997.
- [9] Dodson, E. D., Scale Model Analogy for Icing Tunnel Testing. Boeing Airplane Company, Transport Division, Document No. D66-7976, March 1962.
- [10] Flight Test with Icing Tanker.
<https://www.globalsecurity.org/jhtml/jframe.html#https://www.globalsecurity.org/military/systems/aircraft/images/kc-135r-ait.jpg/>. Accessed: 2019-08-07.
- [11] Fortin, G., Laforte, J. L. and Ilinca, A., Heat and mass transfer during ice accretion on aircraft wings with an improved roughness model. *International Journal of Thermal Sciences*, Vol. 45, p:595-606, 2006.

- [12] Gent, R.W., Dart, N.P. and Cansdale, J.T., Aircraft Icing, Phil. Trans. R. Soc. Lond. A, Vol. 358, p: 2873-2911, 2000.
- [13] Gresho, P. M., Lee, R. L., Sani, R. L., Maslanik, M. K., and Eaton, B. E., The Consistent Galerkin FEM for Computing Derived Boundary Quantities in Thermal and/or Fluid Problems. *International Journal for Numerical Methods in Fluids*, Vol. 7, pp. 371–394, 1987.
- [14] Han, Y., Palacios, J., and Schmitz, S., Scaled ice accretion experiments on a rotating wind turbine blade. *Journal of Wind Engineering and Industrial Aerodynamics*, 109, 55-67, 2012.
- [15] Hauger, H. H. and Englar, K. G., Analysis of Model Testing in an Icing Wind Tunnel, Douglas Aircraft Company, Inc. Report No. SM14933, 1954.
- [16] Hinze. J. O., Turbulence. McGraw-Hill Publishing Co., New York, 1975.
- [17] Hughes, T. J. R., and Brooks, A., A Theoretical Framework for Petrov–Galerkin Methods with Discontinuous Weighting Functions: Application to the Streamline-Upwind Procedure, *Finite Elements in Fluids*, Vol. 4, Wiley, New York, Chap.3, 1982.
- [18] In-flight Icing Test.
<https://www.youtube.com/watch?v=TDyeJ3hcCZY/>. Accessed: 2019-08-07.
- [19] Ice accreted on a Large-Scale Swept Wing Model in the NASA Icing Research Tunnel. <https://www1.grc.nasa.gov/aeronautics/icing/#lightbox-image-0/>. Accessed: 2019-08-07.
- [20] Jackson, E. T., Development Study: The Use of Scale Models in an Icing Tunnel to Determine the Ice Catch on a Prototype Aircraft with Particular Reference to Concord, British Aircraft Corporation (Operating) Ltd., Filton Division, SST/B75T/RMMcK/242, July 1967.
- [21] Junsen Huang, Shuai Nie, Yihua Cao, Yufeng Yao, Jun Yao., Multistep Simulation for Three-dimensional Ice Accretion on an Aircraft Wing.

- [22] Jeck, R. K., Icing Design Envelopes (14 CFR Parts 25 and 29, Appendix C) Converted to a Distance-Based Format (No. DOT/FAA/AR-00/30). FEDERAL AVIATION ADMINISTRATION TECHNICAL CENTER ATLANTIC CITY NJ, 2002.
- [23] Katz, J. and Plotkin, A., *Low-Speed Aerodynamics*, 2nd Ed., Cambridge University Press, 2001.
- [24] Menter, F. R., Two-Equation Eddy-Viscosity Turbulence Models for Engineering Applications, *AIAA J.*, Vol. 32, No. 8, pp. 1598-1605, August 1994.
- [25] Messinger, B. L., Equilibrium Temperature of an Unheated Icing Surface as a Function of Air Speed, *Journal of the Aeronautical Sciences*, 20, pp. 29-42, 1953.
- [26] Myers, T. G., *Extension of the Messinger Model for aircraft icing*, *AIAA J.*, Vol 39, p:211-218, 2001.
- [27] Nakakita, K., Nadarajah, S., and Habashi, W., Toward real-time aero-icing simulation of complete aircraft via FENSAP-ICE. *Journal of Aircraft*, 47(1), 96-109, 2010.
- [28] Özgen, S., Canıbek, M., Ice accretion simulation on multi-element airfoils using Extended Messinger Model, *Heat and Mass Transfer* 45, p. 305-322, 2009.
- [29] Özgen, S., Canıbek, M., Korkem, B. and Ortakaya, Y., Ice shape prediction on airfoils using Extended Messinger method, in 4th Ankara International Aerospace Conference, Ankara, Turkey, 2007.
- [30] Özgen, S., Tarhan, E., Canıbek, M., 3-D in-flight icing simulations and use of parallel computing in Lagrangian droplet trajectory calculations, in 6th Ankara International Aerospace Conference, Ankara, Turkey, 2011.
- [31] Paraschiviou, I., Saeed, F., *Aircraft Icing*, John Wiley & Sons, New York, 2007.
- [32] Pruppacher, Hans R. and Klett, James D., *Microphysics of Clouds and Precipitation*, Reidel, Boston, 1980.

- [33] Raj, L.P., Myong, R.S., Computational Analysis of An Electro-Thermal Ice Protection System in Atmospheric Icing Conditions. *Journal of Computational Fluids Engineering*, 21:1, 1-9, 2016.
- [34] Ruff, G. A., & Dueterhaus, D. A., Analysis and Verification of the Icing Scaling Equations Analysis and Verification, UNITED STATES AIR FORCE, December 1985.
- [35] Sibley, P. J. and Smith, R. E., Jr., Model Testing in an Icing Wind Tunnel. Lockheed Aircraft Corporation, Report No. LRI0981, 1955.
- [36] Wang C., Chang S., Leng M., Wu H., Yang B., A two-dimensional splashing model for investigating impingement characteristics of supercooled large droplets. *International Journal of Multiphase Flow*, 80, 131-149, 2016.
- [37] Wright, W. B., Gent, R. W. and Guffond, D., DRA/NASA/ONERA collaboration on icing research, Part II-prediction of airfoil ice accretion, NASA CR-202349, 1997.
- [38] Yihua Cao, Junsen Huang, Jun Yin., Numerical simulation of three-dimensional ice accretion on an aircraft wing. *International Journal of Heat and Mass Transfer*, 92, 34-54, 2016.
- [39] Zhao Zhan, Wagdi G. Habashi, Marco Fossati., Local Reduced-Order Modeling and Iterative Sampling for Parametric Analyses of Aero-Icing Problems. *AIAA Journal*, 53:8, 2174-2185, 2015.

APPENDICES

A. Mesh and Flow Solution Checks

The mesh that is utilized for computational analysis performed in ANSYS® Fluent 18.0 are given in Figure A.1 and Figure A.2 for NACA0012 and SA13112, respectively.

The boundary layer thickness is adjusted such that the y^+ values are below 1 since the turbulence model $k-\omega$ SST is employed and it is recommended in [4].

The y^+ values are provided in Figure A.3 and Figure A.4. The velocity vectors near wall and near stagnation point are provided in Figure A.5, Figure A.6 for NACA0012 cases and Figure A.7, Figure A.8, Figure A.9, Figure A.10 for SA13112 cases. The cases to check the y^+ values and velocity vectors near the wall are selected considering the lowest Reynolds number since the boundary layer is expected to be thicker in that case to ensure the boundary layer mesh captures the velocity distribution from the wall to the free stream properly.

The y^+ values are below 1 for both airfoils in the lowest Reynolds number cases as it is illustrated in Figure A.3 and Figure A.4.

When the velocity vectors near wall and near stagnation point that are given in Figure A.5, Figure A.6, Figure A.7, Figure A.8, Figure A.9 and Figure A.10 are investigated, it can be concluded that boundary layer mesh captures the velocity distribution properly.

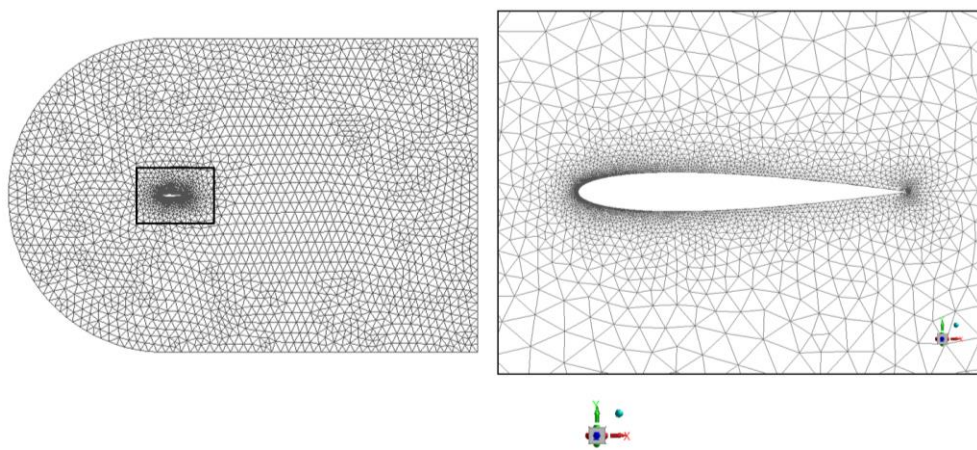


Figure A.1. NACA0012 Mesh

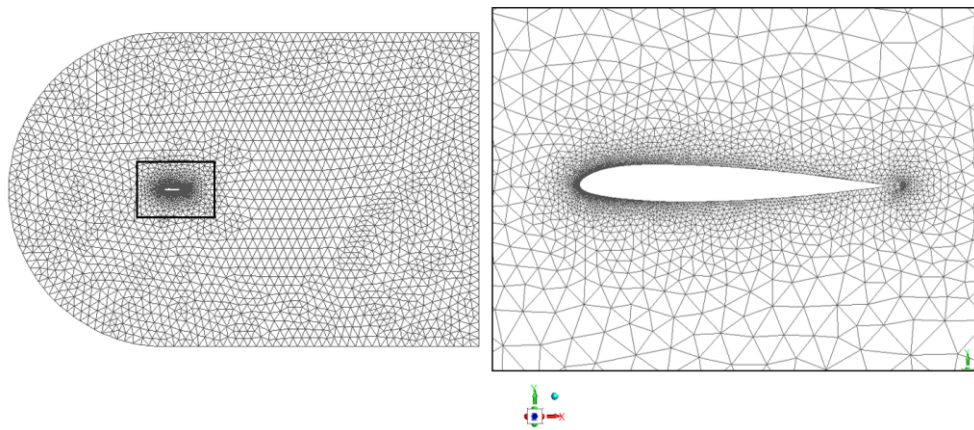


Figure A.2. SA13112 Mesh

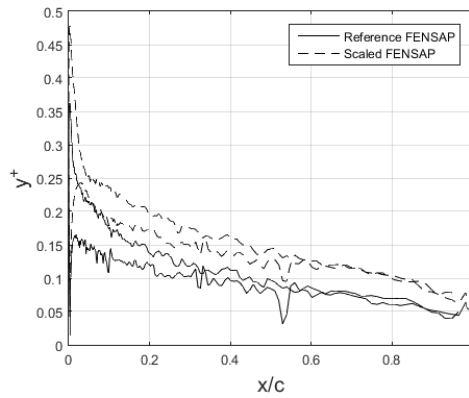
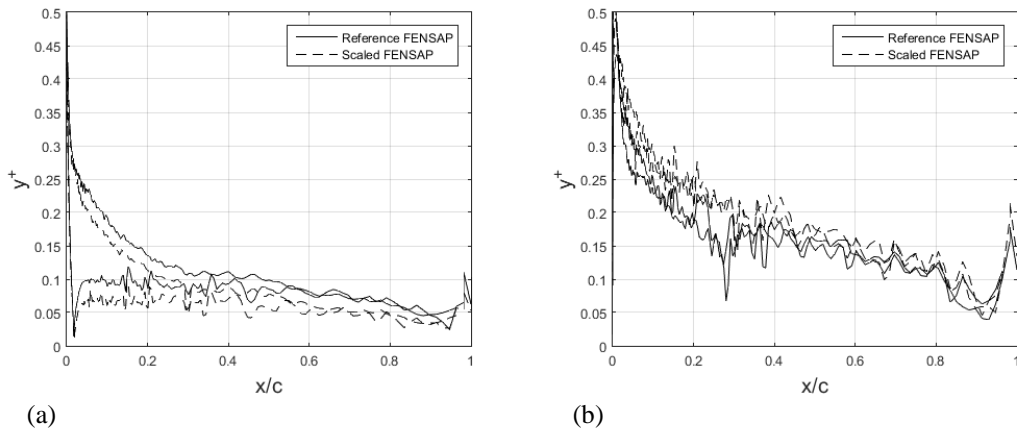


Figure A.3. Case 32 y^+ distributions, NACA0012, $c_{reference}=0.53$ m, $c_{scaled}=0.265$ m



(a) Case 40 y^+ distributions, SA13112, $c_{reference}=0.6$ m, $c_{scaled}=1.2$ m, (b) Case * y^+ distributions, SA13112, $c_{reference}=0.533$ m, $c_{scaled}=0.8$ m

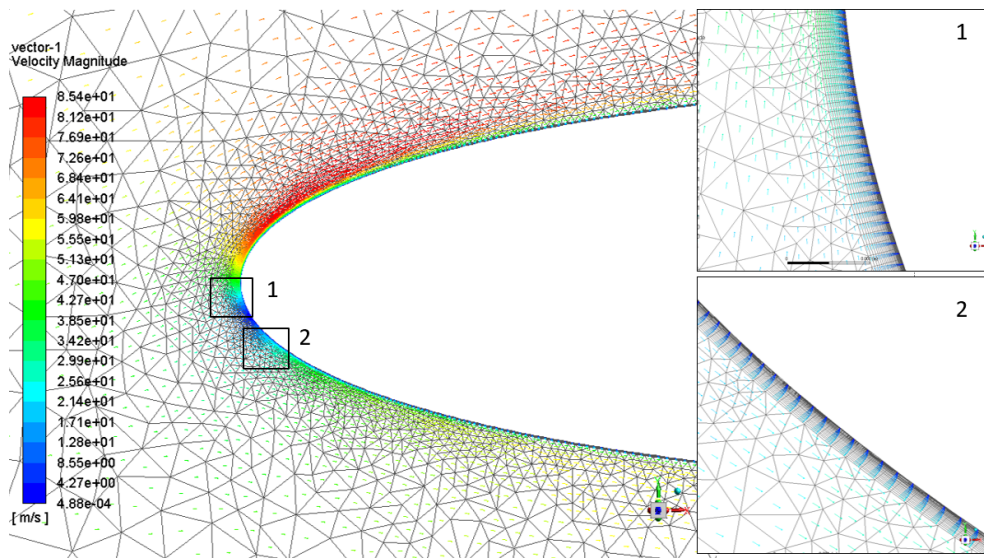


Figure A.5. NACA0012, mesh and velocity vectors in boundary layer for Case 32, $c=0.53$ m

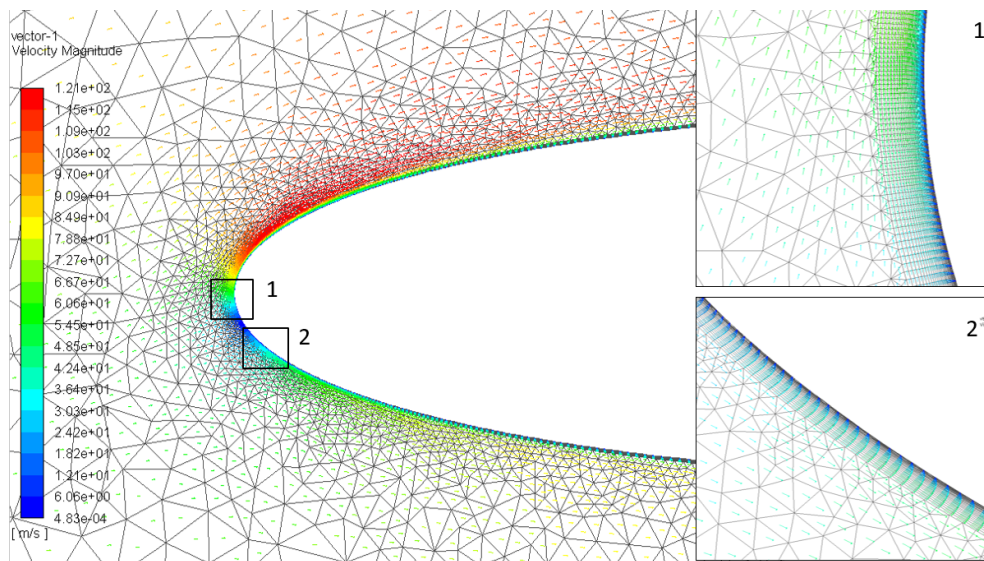


Figure A.6. NACA0012, mesh and velocity vectors in boundary layer for Case 32, $c=0.265$ m

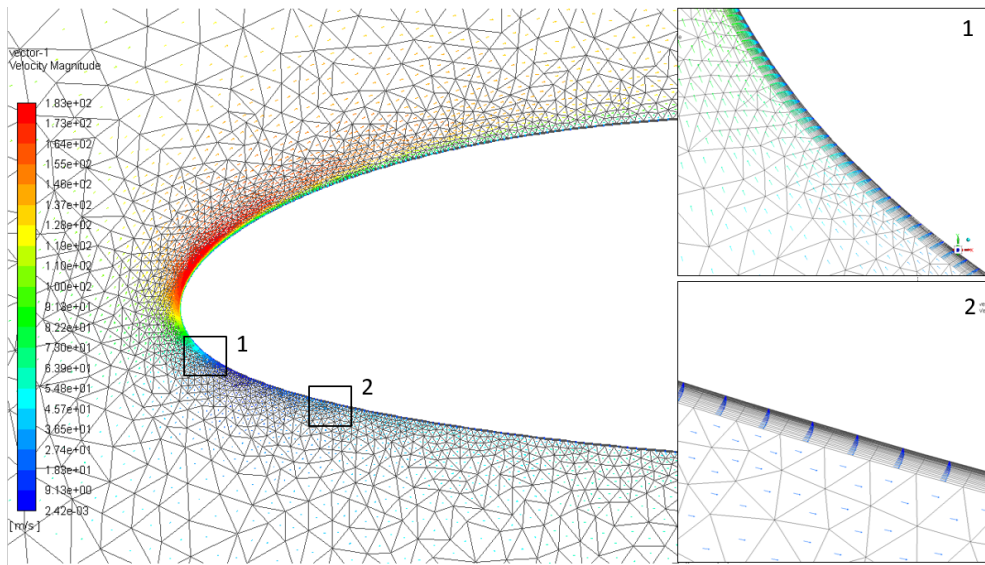


Figure A.7. SA13112, mesh and velocity vectors in boundary layer for Case 40, $c=0.6$ m

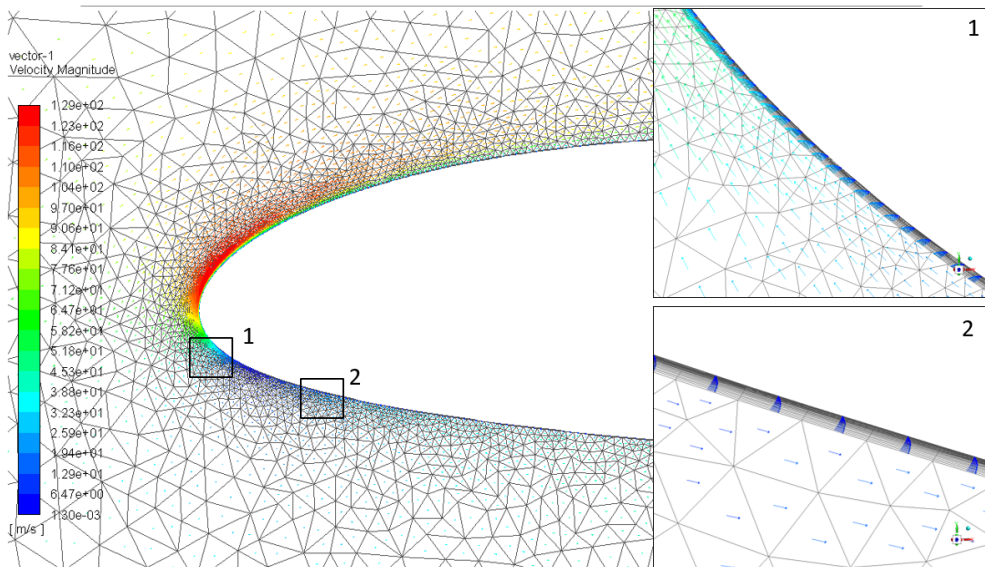


Figure A.8. SA13112, mesh and velocity vectors in boundary layer for Case 40, $c=1.2$ m

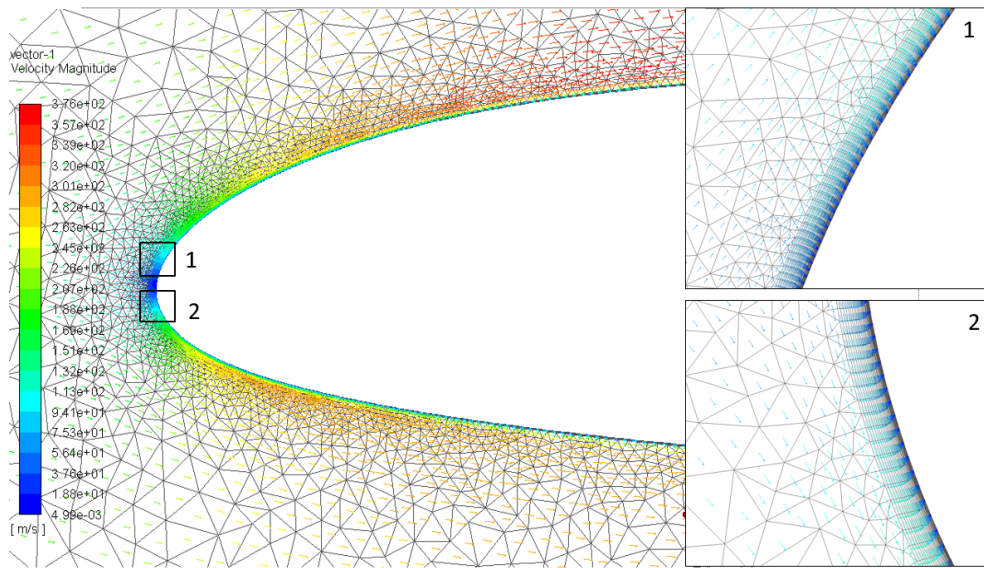


Figure A.9. SA13112, mesh and velocity vectors in boundary layer for Case *, $c=0.533$ m

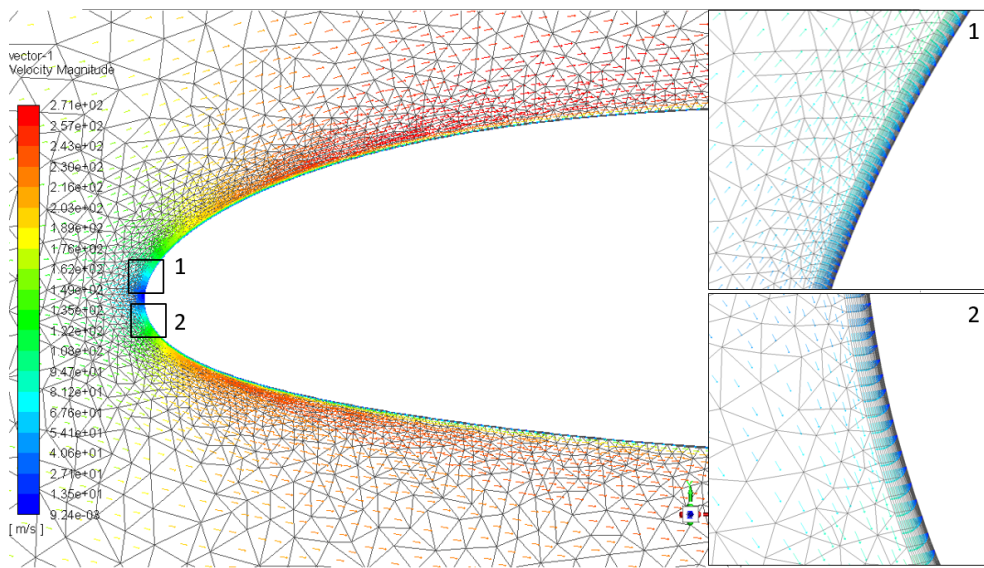


Figure A.10. SA13112, mesh and velocity vectors in boundary layer for Case *, $c=0.8$ m